SYSTEM RELIABILITY ANALYSIS OF STRUCTURES SUBJECTED TO FATIGUE INDUCED SEQUENTIAL FAILURES USING EVOLUTIONARY ALGORITHMS

BY

NOLAN SCOT KURTZ

THESIS

Submitted in partial fulfillment of the requirements
for the degree of Master of Science in Civil Engineering
in the Graduate College of the
University of Illinois at Urbana-Champaign, 2010

Urbana, Illinois

Adviser:

Assistant Professor Junho Song

ABSTRACT

In the past, many catastrophic failures have occurred due to lack of redundancy and managerial oversight. For example, it was found that local failures due to improper welds that connected the suspended truss to the anchor trusses caused the collapse of the Grand Sung-Soo Bridge in Seoul, South Korea on October 21, 1994. Due to a lack of structural redundancy, the initial bridge rib failure was followed by other bridge failures leading to system collapse (Cho et al. 2000). With proper system reliability analysis, such cascading failures could be foreseen by stakeholders. To help make better risk-informed decisions, system reliability methods have been developed to analyze general structures subjected to the risk of cascading system-level failures caused by local fatigue-induced failures. For efficient reliability analysis of such complex system problems, many research efforts have been made to identify critical failure sequences with significant likelihoods by an event-tree search coupled with system reliability analyses: however, this approach is time-consuming or intractable due to repeated calculations of the probabilities of innumerable failure modes, which often necessitates using heuristic assumptions or simplifications. Recently, a decoupled approach was proposed (Kim 2009; Kurtz et al. 2010): critical failure modes are first identified in the space of random variables without system reliability analyses or an event-tree search, then an efficient system reliability analysis (Song & Ok 2010) was performed to compute the system failure probability based on the identified modes. In order to identify critical failure modes in the decreasing order of their relative contributions to the system failure probability, a simulation-based selective searching technique was developed by use of a genetic algorithm. The system failure probability was then computed by a multi-scale system reliability method that can account for the statistical dependence among the component events as well as among the identified failure modes (Song & Kang 2009).

Part of this work presents this decoupled approach in detail and demonstrates its applicability to complex bridge structural systems that are subjected to the risk of cascading failures induced by fatigue. Using a recursive formulation for describing limit-states of local fatigue cracking, the system failure event is described as a disjoint cut-set event (Lee & Song 2010). Critical cut-sets, i.e. failure sequences with significant likelihood are identified by the selective searching technique using a genetic algorithm. Then, the probabilities of the cut-sets are computed by use of crude Monte Carlo simulations. Owing to the mutual exclusiveness of the

cut-sets, the lower-bound on the system cascading failure probability is obtained by a simple addition of the cut-set probabilities. A numerical example of a bridge structure demonstrates that the proposed search method skillfully identifies the dominant failure modes contributing most to the system failure probability, and the system reliability analysis method accurately evaluates the system failure probability with statistical dependence fully considered. An example bridge with approximately 100 truss elements is considered to investigate the applicability of the method to realistic large-size structures. The efficiency and accuracy of the method are demonstrated through comparison with Monte Carlo simulations.

The aforementioned system reliability analysis is based off of an a priori inspection cycle time and computes the probability that the time until the system failure is smaller than the given inspection cycle. Since most field practitioners do not know this value beforehand, a new method has been developed to perform simplified reliability analysis for many performance levels simultaneously. The First-Order Reliability Method (FORM) (see Der Kiureghian 2005 for a review) is often used for structural reliability analysis. The proposed method uses a multi-objective genetic algorithm, called Non-dominated based Sorting Genetic Algorithm II (NSGA II) (Srinivas & Deb 1994) to perform many FORM analyses simultaneously to generate a Pareto Surface of design points. From this Pareto surface, data on cases of "critical but unlikely failures" for short inspection cycle times and cases of "less-critical but highly likely failures" for long inspection cycle times can be found at once. From the nature of this method, this approach is termed as "Multi-Objective" FORM. Part of this work presents this Multi-objective FORM in detail. The applicability of this approach is shown through two numerical examples. The first example is a general situation with few random variables. The second example analyzes a statically indeterminate truss subjected to cyclic loading. Both numerical examples are validated with crude-MCS results and show that the method can find a full Pareto Surface, which provides reliability analysis results at a range of performance levels along with the probability distribution of the performance quantity.

Dedicated to Scot and Karen Kurtz

ACKNOWLEDGEMENTS

Of the many people who have aided me in my quest for knowledge in my first years of grad school, I would like to thank my adviser Professor Junho Song for all of his patience and careful guidance. Without him, I am largely uncertain as to how high the current quality of my research and understanding would be. I would also like to thank my mother and father for all of their support and being there for me. I would lastly like to thank the rest of my family, friends, and especially the new friends I have made at the University of Illinois at Urbana-Champaign for their support and new ideas from other fields.

TABLE OF CONTENTS

CHAPTER 1

INTRODUCTION

1.1 MOTIVATION

There are currently many aging structures that are nearing or have already surpassed their design life. After many disastrous bridge collapses in the last 20 years, designers more than ever need to make proper risk-informed decisions on how and when to inspect and maintain these bridges, as well as where these bridges are most likely to fail. These bridge collapses initiate due to traffic loadings that cause a local component to fail after sufficient time has passed to reduce the cross section of a member via the formation of a large crack. The load is then redistributed and thus causes different cyclic stresses throughout the bridge structure, which may induce progressive member failures toward the system-level collapse of the bridge. These fatigue-induced cascading failures are particularly disastrous because they may occur without much warning and at stress levels well below the yield stresses. A particularly notable example of this type of failure was the collapse of the Grand Sung-Soo Bridge in Seoul, South Korea on October 21, 1994. Due to improper welds that connected the suspension truss to the anchor trusses, local fatigue failures caused one of the bridge ribs to fail (Cho et al. 2000). Due to a lack of structural redundancy, the load the central rib used to support was transmitted to the exterior ribs. Since these were unable to support the new load due to their faulty welds at the same location, these failed immediately, and dropped the full suspended truss in between the 10^{th} and 11^{th} piers. Another catastrophic cascading failure occurred August 1, 2007 when the I-35W Mississippi River Bridge collapsed during evening rush hour traffic (NTSB 2008). Here, an undersized gusset plate at one of the U10 nodes failed due to increased local loading from a bridge deck repaving operations amongst many other issues. The load was then redistributed and due to a lack of structural redundancy an immediate catastrophic bridge collapse occurred. With proper system reliability analysis, such cascading failures could be foreseen by stakeholders. They could then adopt proper inspection and managerial practices to prevent such catastrophes.

1.2 REVIEW OF IMPORTANT CONCEPTS

Before investigating various solutions for the aforementioned issue, several important concepts in the field of structural reliability analysis need to be discussed. Of these issues, system reliability analysis, the first-order reliability method, and operators used in genetic algorithms must be well understood. These specific issues, among others, will be discussed in the following sections.

1.2.1 SYSTEM RELIABILITY ANALYSIS

To complete full system reliability analysis, one must first identify the set of all relevant basic random variables $\mathbf{x} = \{x_1, \ldots, x_n\}^T$ and the subset of the outcomes of these random variables, Ω, which defines the failure event of the system. The probability of the system failure can then be written as the *n*-fold integral

$$P_f = \int_{\Omega} f(\boldsymbol{x}) d\boldsymbol{x} \tag{1}$$

where $f(\mathbf{x})$ is the joint probability density function (PDF) of $\mathbf{x}$. Since it is difficult to evaluate such an integral for general systems which have many random variables, one must seek to find this probability in a more specific manner. Ω is typically characterized by sets of limit state functions present in a system. For a "component" reliability problem, once can define Ω as

$$\Omega = \{g(\boldsymbol{x}) \leq 0\} \tag{2}$$

where $g(\boldsymbol{x})$ is a single limit-state function, which indicates the failure domain by its non-positive sign. For a general "system" reliability problem, one can define Ω as

$$\Omega = \bigcup_k \bigcap_{j \in C_k} \{g_j(\boldsymbol{x}) \leq 0\} \tag{3}$$

where C_k here represents the *k*-th cut-set or failure mode of the system and the $g_j(\mathbf{x})$ represents the *j*-th limit-state function which describes one of the component events contained in C_k. The intersection here represents each cut-set, and, since any of these cut-sets will cause a system failure event, the union describes the system failure event described by the domain Ω. This can also be thought of as a series system of parallel subsystems. Parallel systems define Ω as

$$\Omega = \bigcap_k \{g_k(\boldsymbol{x}) \leq 0\} \quad (4)$$

Here, all component events must occur at once to characterize a system failure. A good example of this kind of system is an assembly of electrical equipment items located in parallel. All equipment items must fail before the assembly can lose the connectivity. On-the-other-hand, series systems define Ω as

$$\Omega = \bigcup_k \{g_k(\boldsymbol{x}) \leq 0\} \quad (5)$$

Here, the occurrence of at least one of the component events constitutes a system failure. A good example of this kind of system is flow through a long pipeline. If the pipe fails at any point along the pipe, the system does not deliver full flow anymore and is said to have failed. This type of system could also be a statically-determinate structure, where a single component failure causes loss of global stability. Once one has characterized Ω and the associated limit-state functions, one can obtain P_f in (1) through many methods. Of these many choices, the most standard and efficient methods available are the First- and Second- Order Reliability Method (FORM and SORM) (see Der Kiureghian 2005 for a review). These are particularly applicable to component reliability problems in (2). Other possible methods for system reliability analysis are sampling based methods such as Monte-Carlo Simulation and Importance Sampling, which will be described in Section 1.2.5, and response surface methods.

1.2.2 NONLINEAR TRANSFORMATION TO THE SPACE OF UNCORRELATED STANDARD NORMAL SPACE

To perform FORM and SORM analysis with non-normal random variables, one must first use a nonlinear transformation to transform the space of the original random variables, **x** to that of standard normal uncorrelated random variables, **u**. Such a transformation will be designated as $\mathbf{u} = \mathbf{T}(\mathbf{x})$ and exists as long as the joint cumulative density function (CDF) of **x** is continuous and is strictly increasing for each random variable in **x**. For FORM and SORM, the inverse transform $\mathbf{x} = \mathbf{T}^{-1}(\mathbf{u})$ and the Jacobian of **T**, $\mathbf{J}_{\mathbf{u},\mathbf{x}}$, are also needed. This transformation can be defined for four different types of situations, depending on the types of and the correlations between random variables in **x**: (1) statistically independent random variables, (2) dependent normal random variables, (3) Nataf distributed random variables, and (4) dependent non-normal,

non-Nataf random variables, as outlined by Der Kiureghian (2005). Since most cases encountered generally have non-normal random variables and have dependence, the Nataf distributed random variables will be discussed here. Since the Nataf distribution is much more applicable than the non-Nataf class, the last case will not be included in this discussion.

Suppose, for a given set of statistically dependent random variables $\mathbf{x} = \{x_1, \ldots, x_n\}$, $i = 1, \ldots, n$, their marginal CDFs $F_i(x_i)$ and correlation coefficients ρ_{ij}, $i,j = 1, \ldots, n$ are given. Then, a Nataf distribution can be constructed via correlated standard normal random variables

$$z_i = \Phi^{-1}[F_i(x_i)] \qquad i = 1, 2, \ldots, n \tag{6}$$

where $\Phi^{-1}[\cdot]$ denotes the marginal inverse CDF of the standard normal distribution. The correlation coefficients for the set of correlated standard normal random variables, $\mathbf{z}$, can be found through the relationship (Liu & Der Kiureghian 1986)

$$\rho_{ij} = \int_{-\infty}^{\infty} \int_{-\infty}^{\infty} \left(\frac{x_i - \mu_i}{\sigma_i}\right) \left(\frac{x_j - \mu_j}{\sigma_j}\right) \varphi_2(z_i, z_j, \rho_{0,ij}) dz_i dz_j \tag{7}$$

where μ_i and σ_i are the mean and standard deviation of x_i, ρ_{ij} is the correlation coefficient between x_i and x_j, $\rho_{0,ij}$ is the correlation coefficient between z_i and z_j, and $\varphi_2(z_i, z_j, \rho_{0,ij})$ is the bivariate normal PDF for z_i and z_j. Given that the marginal CDFs for all random variables in $\mathbf{x}$ were continuous and monotonically increasing and the correlation matrix $\mathbf{R} = |\rho_{ij}|$ is positive-definite, the Nataf distribution is valid given that $\mathbf{R}_0 = |\rho_{0,ij}|$ is a valid correlation coefficient matrix. The required transformation to obtain $\mathbf{u}$ is then given by

$$\mathbf{u} = \mathbf{L}_0^{-1} \begin{Bmatrix} \Phi^{-1}[F_1(x_1)] \\ \vdots \\ \Phi^{-1}[F_n(x_n)] \end{Bmatrix} \tag{8}$$

where $\mathbf{L}_0$ is the lower-triangular matrix obtained by Choleski decomposition of the correlation matrix $\mathbf{R}_0$. This completes the nonlinear transformation $\mathbf{u} = \mathbf{T}(\mathbf{x})$. On the other hand, the inverse transformation $\mathbf{x} = \mathbf{T}^{-1}(\mathbf{u})$ consists of finding the correlated standard normal variables $\mathbf{z} = \mathbf{L}_0\mathbf{u}$ and $x_i = F_i^{-1}[\Phi(z_i)]$, $i = 1, \ldots, n$.

The Jacobian for the transformation $\mathbf{u} = \mathbf{T}(\mathbf{x})$, i.e. $\mathbf{J_{u,x}}$, is evaluated by $\mathbf{J_{u,z}} \cdot \mathbf{J_{z,x}}$ where $\mathbf{J_{u,z}}$ is just $\mathbf{L}_0^{-1}$ from (7), and $\mathbf{J_{z,x}}$ is a diagonalized matrix with terms

$$J_{ii} = \frac{f_i(x_i)}{\varphi(z_i)} \qquad i = 1, 2, \dots, n \tag{9}$$

where $\varphi(\cdot)$ denotes the univariate standard normal PDF.

1.2.3 THE FIRST-ORDER RELIABILITY METHOD

To simplify the component reliability analysis problem in (1) with (2), the first-order reliability method (FORM) linearizes the limit state function at the most likely point in the failure domain, which will be referred to as the design point in this discussion. The only requirement for FORM is that the limit states be continuous and differentiable in the neighborhood of the design point. If (1) is transformed to the standard normal uncorrelated space as discussed in the previous section and applied for a component reliability analysis is shown in (2), the equation becomes

$$P_f = \int_{\mathbf{g(x)} \le 0} f(\mathbf{x}) d\mathbf{x} = \int_{G(u) \le 0} \varphi_n(\mathbf{u}) d\mathbf{u} \tag{10}$$

where $G(\mathbf{u}) = g(\mathbf{T}^{-1}(\mathbf{u}))$. To perform FORM, $G(\mathbf{u})$ must be linearized about the design point $\mathbf{u}^*$, which is found by solving the constrained optimization problem

$$\mathbf{u}^* = \arg\min\{\|\mathbf{u}\| | G(\mathbf{u}) = 0\} \tag{11}$$

where "arg min" represents the argument of the minimum of the designated function. Since $G(\mathbf{u}^*) = 0$, one can see that $\mathbf{u}^*$ must be located on the limit state surface and have the minimum distance from the origin in the standard normal uncorrelated space as shown in Figure 1.1. Since the probability density decreases exponentially in the radial direction from the origin, and decreases exponentially in the tangential direction orthogonal to the location of a given point with reference to the origin, one can say $\mathbf{u}^*$ has the highest probability density among all other outcomes of the limit state function $G(\mathbf{u}) \le 0$, and the vicinity around $\mathbf{u}^*$ contributes most to the integral in (10).

To linearize $G(\mathbf{u})$ about $\mathbf{u}=\mathbf{u}^*$, one can use

$$G(\mathbf{u}) \cong \nabla G(\mathbf{u}^*)(\mathbf{u}-\mathbf{u}^*) = \|\nabla G(\mathbf{u}^*)\|(\beta - \hat{\boldsymbol{\alpha}}\mathbf{u}) \tag{12}$$

where $\nabla G(\mathbf{u}) = [\frac{\partial G}{\partial u_1}, \dots, \frac{\partial G}{\partial u_n}]$ denotes the gradient row vector, $\hat{\boldsymbol{\alpha}} = -\nabla G(\mathbf{u}^*)/\|\nabla G(\mathbf{u}^*)\|$ is the normalized negative gradient row vector at the design point which point toward the failure domain, and $\beta = \hat{\boldsymbol{\alpha}}\mathbf{u}^*$ is the reliability index. This linearization replaces $G(\mathbf{u}) \leq 0$ by the half space $\beta - \hat{\boldsymbol{\alpha}}\mathbf{u}^* \leq 0$, as shown in Figure 1.1. The first-order approximation of the failure probability is given by the probability in the hyperspace completely defined by the distance β in the $\mathbf{u}$ space; therefore,

$$P_f \cong P_{f1} = \Phi(-\beta) \tag{13}$$

where the 1 subscript denotes a first-order approximation. FORM is usually an appropriate approximation unless two situations occur: there are large curvatures at the location of $\mathbf{u}^*$, or there are multiple local or global solutions to (11). To address the issues of curvatures, SORM or importance sampling may be used. The second condition may be addressed using multiple linearizations, a more theoretically rigorous method or as described in Der Kiureghian & Dakessian (1998).

To perform FORM analysis, the main computational effort is oriented toward solving (11). One well-proven method to perform this optimization uses an iterative algorithm such as

$$\mathbf{u}_{i+1} = \mathbf{u}_i + \lambda_i \mathbf{d}_i \qquad i = 1,2, \dots \tag{14}$$

where $\mathbf{d}_i$ is the search direction vector and λ_i is a step size. There are many ways to choose $\mathbf{d}_i$ and λ_i, but a choice that applies to many problems is the one proposed by Hasofer and Lind and later generalized by Rackwitz and Fissler

$$\mathbf{d}_i = \left[\frac{G(\mathbf{u}_i)}{\|\nabla G(\mathbf{u}_i)\|} + \hat{\boldsymbol{\alpha}}_i \mathbf{u}_i\right] \hat{\boldsymbol{\alpha}}_i^{\mathrm{T}} - \mathbf{u}_i \tag{15}$$

This method will not converge with $\lambda_i = 1$ when the principal curvature of the limit state surface satisfies $1 \leq |\beta\kappa_i|$ where κ_i is a principal curvature at the design point. By monitoring a

merit function, $m(\mathbf{u})$, λ_i can be selected appropriately. The merit function is any continuous and differentiable function of $\mathbf{u}$ whose minimum coincides with the design point and the value decreases when the algorithm moves along $\mathbf{d}_i$ starting from $\mathbf{u}_i$. Zhang and Der Kiureghian (1995) have shown that a good choice of merit function is

$$m(\mathbf{u}) = \frac{1}{2}\|\mathbf{u}\|^2 + c|G(\mathbf{u})| \tag{16}$$

where c is the penalty parameter and must be selected at each step to ensure $c_i > \|\mathbf{u}_i\| / \|\nabla G(\mathbf{u}_i)\|$. It is sufficient to select $\lambda_i \in (0,1]$ such that $m(\mathbf{u}_i + \lambda \mathbf{d}_i) < m(\mathbf{u}_i)$ for the suggested algorithm above. This suggested method is well known as the HL-RF algorithm. Since the limit state function and its gradient are only known in the original space of random variables, the gradient and function value must be found for the $\mathbf{u}$ space to calculate the terms in (11), (12), (15), and (16). Since the transformation $\mathbf{x}_i = \mathbf{T}^{-1}(\mathbf{u}_i)$ is known, it follows that $G(\mathbf{u}_i) = g(\mathbf{x}_i)$ and $\nabla G(\mathbf{u}_i) = \nabla g(\mathbf{x}_i)\mathbf{J}_{\mathbf{u},\mathbf{x}}^{-1}(\mathbf{x}_i)$.

1.2.4 FORM IMPORTANCE MEASURES

Once FORM analysis has finished, information about the relative importance of individual random variables can be obtained. Analyzing the transformed linearized limit-state function in the $\mathbf{u}$ space in (12), and remembering that the covariance matrix is the identity matrix along with the mean of $\mathbf{u}$ being a zero vector, the mean and variance of $G_1(\mathbf{u})$, the linearized approximation of $G(\mathbf{u})$ as shown by $\beta - \hat{\boldsymbol{\alpha}}\mathbf{u}$ in (12), are

$$\mu_{G_1} = \|\nabla G\|\beta \tag{17}$$

$$\sigma_{G_1}^2 = \|\nabla G\|^2(\hat{\alpha}_1^2 + \hat{\alpha}_2^2 + \cdots + \hat{\alpha}_n^2) = \|\nabla G\|^2 \tag{18}$$

where (18) implements the fact that the vector $\hat{\boldsymbol{\alpha}}$ is a unit vector. From this information, one can clearly see that $\beta = \frac{\mu_{G_1}}{\sigma_{G_1}}$, guaranteeing that the reliability index is the one for the linearized limit state, $G_1(\mathbf{u})$, and that the squared contributions of the alpha vector are proportional to the contribution of the standard normal uncorrelated random variables to the variance of the limit state function. The larger this contribution, the more important the random variable u_i is;

therefore, $\hat{\boldsymbol{\alpha}}$ provides a relative importance measure for each u_i, $i = 1,\ldots,n$. From the expanded linearized limit-state function, $G_1(\mathbf{u}) = \|\nabla G\|(\beta - \alpha_1 u_1 - \cdots - \alpha_n u_n)$, one can see that positive values of α indicate load type random variables and negative values of α indicate capacity type random variables.

Since significant correlation exists between random variables in most systems, obtaining relative importance of the original random variables, $x_i, i = 1, \ldots, n$, is preferred, since the importance vector for **u** will not reflect the effects of correlation. To model correlation effects, linearize the nonlinear transformation **u** = **T**(**x**) at the design point

$$\mathbf{u} \cong \mathbf{u}^* + \mathbf{J}_{\mathbf{u},\mathbf{x}}(\mathbf{x} - \mathbf{x}^*) \tag{19}$$

For the purposes of this discussion, denote the value of **x** satisfying (19) by $\hat{\mathbf{x}}$. $\hat{\mathbf{x}}$ can be considered as an approximation of **x** that corresponds to a given **u** based on the linear transform in (19). Since **u** is a linear function of $\hat{\mathbf{x}}$, $\hat{\mathbf{x}}$ must be jointly normal, making the covariance matrix of $\hat{\mathbf{x}}$

$$\hat{\Sigma} = \mathbf{J}_{\mathbf{u},\mathbf{x}}^{-1}\left(\mathbf{J}_{\mathbf{u},\mathbf{x}}^{-1}\right)^{\mathrm{T}} \tag{20}$$

One can see from (20) that $\hat{\Sigma}$ is different from the original covariance matrix Σ since it depends on the linear approximation at the design point and that the magnitude of this difference depends on the non-normality of **x**. $\hat{\mathbf{x}}$ can then be called the "equivalent normals" of **x** at the design point. If (20) is substituted into (19) using $\hat{\mathbf{x}}$, the first order limit state function described in (12) is redefined as:

$$G_1(\mathbf{u}) = -\|\nabla G\|\hat{\boldsymbol{\alpha}}\mathbf{J}_{\mathbf{u},\mathbf{x}}(\hat{\mathbf{x}} - \mathbf{x}^*) \tag{21}$$

From (12), the variance is described in terms of the equivalent normals as follows.

$$\sigma_{G_1}^2 = \|\nabla G\|^2\left(\hat{\boldsymbol{\alpha}}\mathbf{J}_{\mathbf{u},\mathbf{x}}\hat{\Sigma}\mathbf{J}_{\mathbf{u},\mathbf{x}}^T\hat{\boldsymbol{\alpha}}^{\mathrm{T}}\right) = \|\nabla G\|^2\left(\left\|\hat{\boldsymbol{\alpha}}\mathbf{J}_{\mathbf{u},\mathbf{x}}\hat{\mathbf{D}}\right\|^2 + \hat{\boldsymbol{\alpha}}\mathbf{J}_{\mathbf{u},\mathbf{x}}(\hat{\Sigma} - \hat{\mathbf{D}}\hat{\mathbf{D}})\mathbf{J}_{\mathbf{u},\mathbf{x}}^T\hat{\boldsymbol{\alpha}}^{\mathrm{T}}\right) \tag{22}$$

where $\hat{\mathbf{D}}$ is the diagonal matrix of standard deviations of $\hat{\mathbf{x}}$. The first portion of 22 accounts for the individual variances of the elements of $\hat{\mathbf{x}}$, whereas the second term accounts for the statistical

dependencies between elements of $\hat{\mathbf{x}}$; therefore, elements of $\hat{\boldsymbol{\alpha}}\mathbf{J}_{\mathbf{u},\mathbf{x}}\hat{\mathbf{D}}$ provides relative importance measures of the equivalent normals, and approximately of the original random variables. Normalizing this vector, one obtains

$$\hat{\boldsymbol{\gamma}} = \frac{\hat{\boldsymbol{\alpha}}\mathbf{J}_{\mathbf{u},\mathbf{x}}\hat{\mathbf{D}}}{\left\|\hat{\boldsymbol{\alpha}}\mathbf{J}_{\mathbf{u},\mathbf{x}}\hat{\mathbf{D}}\right\|} \tag{23}$$

where $\hat{\boldsymbol{\gamma}}$ is defined as the relative importance vector of the random variables $\mathbf{x}$. The meaning of the signs for $\hat{\boldsymbol{\alpha}}$ also holds for $\hat{\boldsymbol{\gamma}}$.

1.2.5 IMPORTANCE SAMPLING

As described previously, sometimes, due to high nonlinearities in the limit state functions, it becomes necessary to use a method other than FORM to estimate the failure probability. Importance sampling is one of these alternatives. A good summary of importance sampling is described by Melchers (1999). To start, consider the basic equation of crude-Monte Carlo Simulation (MCS) beginning from 1:

$$p_f = \int_{\Omega} I[g(\mathbf{x}) \leq 0] f_{\mathbf{X}}(\mathbf{x}) d\mathbf{x} \tag{24}$$

where $I[\ ]$ is the "indicator function" which is equal to 1 when the expression between the brackets is true and 0 when the expression is untrue, and $f_{\mathbf{X}}(\mathbf{x})$ is the joint PDF of the original random variables. If N samples of $\mathbf{x}$ are generated, 24 becomes:

$$\hat{p}_f = \frac{1}{N}\sum_{i=1}^{N} I[g(\hat{\mathbf{x}}_i) \leq 0] = E[I[g(\hat{\mathbf{x}}) \leq 0]] \tag{25}$$

It is clear that for a large enough sample, (25) provides an accurate, direct estimate of (1).

The size of the sample can be determined such that one can achieve a level of the coefficient of variation (COV, or $\delta_{p_{\mathbf{X}}}$) of the estimate $\hat{p}_f$. $\delta_{p_{\mathbf{X}}}$ is defined as the ratio of the standard deviation to the mean of the estimate. First, the mean is defined as:

$$E[\hat{p}_{\mathbf{X}}] = \frac{1}{N}\sum_{i=1}^{N} E\left[I[g(\hat{\mathbf{x}}_i) \leq 0]\right] = \frac{1}{N}\sum_{i=1}^{N} \hat{p}_{\mathbf{X}} = \hat{p}_{\mathbf{X}} \tag{26}$$

Second, the variance of the estimate is then defined as:

$$Var[\hat{p}_{\mathbf{X}}] = \frac{1}{N^2}\sum_{i=1}^{N} Var\left[I[g(\hat{\mathbf{x}}_i) \leq 0]\right] \tag{27}$$

Using the fact that the value of the index function *I* is a Bernoulli random variable,

$$Var[\hat{p}_{\mathbf{X}}] = \frac{1}{N^2}[N\hat{p}_{\mathbf{X}}(1-\hat{p}_{\mathbf{X}})] = \frac{\hat{p}_{\mathbf{X}}(1-\hat{p}_{\mathbf{X}})}{N} \tag{28}$$

then, $\delta_{p_{\mathbf{X}}}$ is determined as:

$$\delta_{p_{\mathbf{X}}} = \sqrt{\frac{\hat{p}_{\mathbf{X}}(1-\hat{p}_{\mathbf{X}})}{N}}\frac{1}{\hat{p}_{\mathbf{X}}} = \sqrt{\frac{(1-\hat{p}_{\mathbf{X}})}{\hat{p}_{\mathbf{X}}N}} \tag{29}$$

For example, if the probability desired is around 10^{-2}, then around one million samples are need for $\delta_{p_{\mathbf{X}}} = 0.01$. For smaller probabilities, much larger sample sizes are required, making crude-MCS an improper method for efficient, quick estimates of the failure probabilities.

To improve efficiency, various importance sampling methods have been developed. The basis of importance sampling is similar to (24):

$$p_f = \int_{\Omega} I[g(\mathbf{x}) \leq 0]\frac{f_{\mathbf{X}}(\mathbf{x})}{h_v(\mathbf{x})}h_v(\mathbf{x})d\mathbf{x} \tag{30}$$

where $h_v(\mathbf{x})$ is the "importance sampling" PDF and is selected based off of knowledge about the problem. If *N* samples of **x** are generated from $h_v(\mathbf{x})$, (30) becomes

$$p_f = \frac{1}{N}\sum_{i=1}^{N}\left\{I[g(\mathbf{x}) \leq 0]\frac{f_{\mathbf{X}}(\mathbf{x})}{h_v(\mathbf{x})}\right\} \tag{31}$$

where it is obvious that the function of $h_v(\mathbf{x})$ is to scale the sampling such that much less samples are required. Many choices are available for $h_v(\mathbf{x})$, but a dependable one is the jointly-Normal uncorrelated PDF about the design point, **u***, in the **u** space, if **u*** is known. The mean of this PDF will be **u***. While the covariance matrix for these variables in the **u** space will have zero correlations, the standard deviations (the square-root of the diagonal elements) may not be simply one, as expected for normal PDFs in the **u** space. These values must be selected

appropriately with two notes of caution: standard deviations which are too small will cause the method to converge quickly to an incorrect value, and if they are too large, they will lose lots of efficiency. Importance sampling can improve the accuracy of FORM especially when high non-linearity of the limit-state function exists.

1.2.6 GENETIC OPERATORS

The two reliability methods developed in this thesis make use of genetic algorithm search. A proper summary of Genetic Algorithm search can be found in Holland (1975) and Goldberg (1989). This family of search algorithms are simulation-based searching techniques that require each data point be represented in a *chromosome*. The initial chromosomes are generated randomly or may be created in such a way to reflect the application. In this use, chromosomes are generated based off of knowledge about the random variables needed. These chromosomes consist of *alleles*, or individual data. In other words, **x** is an array of individual values of random variables x_i's, where **x** is a chromosome and x_i is an allele value. A certain number of chromosomes are usually specified a priori using either a developed rule or the executor's discretion. This is so-called population number. Once the population has been sampled, the chromosomes must be ranked to find which chromosomes will be in the *mating pool*. Genetic algorithms require the use of a *fitness function* to characterize which chromosomes are *elite*. A good example of a fitness function in the realm of structural reliability would be the event of a system failure, i.e. if a certain array of random variable values leads to a system failure. The use of elite here means that these chromosomes are most likely to pass their allele data to the *offspring* population. This offspring population will then become the next *generation* of parent chromosomes.

The offspring population is then developed through many possible ways, but, in most applications, one can expect to use two basic operators: *crossover* and *mutation*. Both of these require a certain probability of occurrence. Crossover can occur in many different ways, but typically a random number is generated to select a parent that will submit its allele data first or dominate a given receiving offspring's allele data. Allele data may be interchanged as whole numbers or with a weighted average in the child chromosomes. There may be a single crossover point where allele data is exchanged in aggregate between two parent chromosomes to create a

child; on-the-other-hand, allele data may be from either parent alternating throughout the child chromosome. Since crossover typically helps the genetic algorithm converge, it typically has a high probability value, on the order of 90% to 100% in most applications. One can lower this value to keep certain high fitness chromosomes always present in the mating pool without modification to individual alleles, but this may or may not adversely affect the computational effort of the algorithm. The purpose of crossover is to search within the identified domains of high-fitness the chromosomes. One can think of this process as if two particular failure modes are identified that are associated to two parent chromosomes, crossover develops two offspring that are in the domain of the original chromosomes, finding other similar failure modes. This is best visualized in the standard normal uncorrelated space of random variables as seen in Figure 1.2. If one parent chromosome is found in failure mode 1 and one in failure mode 3, a crossover operation may have an offspring in failure mode 2.

An important point to remember when using genetic algorithms is that they are sensitive to premature convergence if proper actions are not taken to force the methods to search deeper. To fix this issue, *mutation*, i.e. random changes to allele data in offspring, was developed. Mutation is typically applied after crossover, but may also be used interchangeably with crossover depending on the application. It can be implemented in many ways, but typically it is some sort of quantifiable random change to a given allele, whether it be a sign inversion, scaling, or addition. Since this genetic operator tends to redirect the genetic algorithm from its original searching path, causing higher computing times, it is usually assigned a low probability of occurrence, e.g. 30%. This is meant to mimic mutations in biological populations, where mutations typically are rare. In this mathematical realm, mutation is meant to search for high fitness chromosomes not present in the parent population. In system reliability in particular, mutation searches for failure modes not near the vicinity of those previously identified. For example, if, in the situation proposed by Figure 1.2, all most elite chromosomes indicate failure mode 1, mutation will help future generations identify the other two failure modes, stopping the genetic algorithm from converging prematurely.

One last method for determining the next population is *leeching*. Leeching is a process where past populations are saved and compared to current generations. If higher fitness function values are found in past populations, these are then given preference and placed into the next

generation. The members of the current population that have the worst fitness function values are replaced by these past dominant chromosomes from past populations. Leeching can be implemented in many ways. This operation helps genetic algorithms to converge quickly; however, one must not forget that genetic algorithms must not converge too quickly, or else an incorrect solution may be found. Leeching must only be used in appropriate situations. This process of generating new generations is repeated until some convergence criteria are met, but these are highly dependent on the exact application.

1.3 RESEARCH OBJECTIVES

To address concerns that arise from the issues discussed in Section 1.1, several research initiatives have occurred. These technical challenges and several solutions to these are presented in the next section. Lastly, the overall organization of this paper will be discussed.

1.3.1 TECHNICAL CHALLENGES AND SOLUTIONS

In past research efforts, the failure probabilities of structural systems have been characterized through component reliability analysis (Freudenthal et al. 1966; Thoft-Christensen & Baker 1982; Ditlevsen & Madsen 1996; Melchers 1999; Der Kiureghian 2005), which describes the system failure event by a single limit state; however, many have concurred that the complexity of a system-level failure may require system reliability analysis (Lee 1989; Moses 1990; Park 2001; Song & Der Kiureghian 2003; Liu & Tang 2004), where the failure event is described as a Boolean function of multiple limit state functions. If this system event were described as a cut-set system,

$$E_{sys} = \cup_{k=1}^{Ncut} C_j = \cup_{k=1}^{Ncut} \left[\cap_{i \in I_{C_j}} E_i \right] \tag{32}$$

where E_i is the *i*-th component failure event representing the failure at a location or member, $i = 1,\ldots,N_{comp}$; C_j is the *j*-th cut-set event, i.e. a failure mode, $j = 1,\ldots, N_{cut}$, where a cut-set is defined as a joint realization of component events that constitutes a realization of the system event N_{sys}; and I_{C_j} is the set of the indices of the components that appear in the *j*-th cut-set.

Component failure events, E_i's are usually statistically dependent on each other due to correlated or common random variables present in the limit state definition (Galambos 1990; Henwadi & Frangopol 1994). For similar reasons, cut-set events C_j are also statistically dependent since they share common or statistically dependent component events. Therefore, an accurate system reliability analysis method must account for statistical dependence among component and failure mode events to evaluate the system-level risk. For efficient system reliability evaluation, most of the existing failure-mode-based approaches employ approximation methods such as bounding formulas (Ditlevsen 1979; Feng 1989; Park 2001) or response surfaces (Zhao & Ono 1998). While these enable rapid system-level risk estimation, there are not flexible in including different types and amounts of available information or in accounting for statistical dependence. A new bounding approach using linear programming (Song & Der Kiureghian 2003) was developed to overcome these issues and was further developed for multi-scale analysis (Der Kiureghian & Song 2008); however, solving such linear programming problems may cause computational or numerical issues when the feasible domain is small or the system event consists of a large number of component events.

Another major issue in system reliability analysis is that innumerable failure modes often exist, due to high degrees of redundancy in real structures and the redefinition of remaining component limit-states once stress has redistributed after a component failure. Stress redistribution and high-redundancy make it difficult to find all possible limit states for system reliability analysis, particularly for complex structures with large numbers of structural elements. To overcome these difficulties, some methods using an event tree (Murotsu et al. 1984; Karamchandani 1987; Srividya & Ranganathan 1992) have been developed to identify only the failure modes with significant likelihoods (Moses & Stahl 1978; Murotsu et al. 1984; Thoft-Christensen & Murotsu 1986; Ranganathan & Deshpande 1984). The system failure probability can then be obtained using identified failure mode probabilities and statistical dependencies; however, while evaluating these individual failure mode contributions in the search process, large amounts of component and system reliability analyses must be performed, requiring high computational cost for structures with large amounts of redundancy.

To deal with such computational cost issues, Kim (2009) proposed a new framework for risk assessment that decouples the identification of the dominant failure mode from evaluation of

the system and failure mode event probabilities. This dichotomy reduces the need for large amounts of component and system reliability analyses in the failure mode searching process. First, dominant failure modes are obtained by a simulation-based selective searching technique inspired by genetic algorithm search, which identifies the dominant failure modes rapidly. These failure mode and system failure probabilities are then evaluated by system reliability analyses. While the system failure probability can be found by brute-force Monte-Carlo simulations given sufficient convergence time, this proposed selective searching method not only identifies the system failure probability but also the critical failure mode probability without prior system response knowledge. In this work, the proposed framework is applied directly and demonstrated for structures subjected to fatigue-induced sequential failures.

When dealing with fatigue-induced sequential failures, since the component failures happen in the time domain, one must specify an inspection cycle time, or time between the proper inspections of the structure's performance. This inspection cycle time is often unknown a priori and based largely on precedence without proper risk-informed decision making. To help allay some of arbitration that is used for selecting an inspection cycle time, a new approach is proposed to find the system reliability for a range of given inspection cycle times simultaneously. While one could obtain such information from FORM or SORM, this approach, through the use of search inspired by the Non-dominated Genetic Algorithm II, does not rely on gradients to find the design points and does not need to repeat itself at many inspection cycle times. This approach is especially helpful when not much prior information about the system is available, since choosing the points for FORM analysis are limited by knowing which inspection cycle times are unrealistically large and small. FORM may also be misled by local gradients to find a local optimal solution instead of the desired global solution for the design point. Since this method does what FORM would do for many different points simultaneously, this method will be called Multi-Objective First-Order Reliability Method (MO-FORM).

1.3.2 ORGANIZATION

For this thesis, the proposed selective searching method is applied to a bridge structural system subjected to the risk of fatigue-induced cascading failures. Using an efficient characterization of fatigue-induced failure modes developed by Lee & Song (2010), cascading

failure events are described as mutually exclusive (or disjoint cut-set events), making the system failure probability simply a sum of the probabilities of all identified critical failure modes. This thesis first introduces the simulated based selective searching technique, followed by a summary of the efficient formulation of fatigue-induced failure modes and methods used for calculating the probability of identified cut-sets. The proposed risk assessment framework is then demonstrated by a large-size planar truss bridge structure. Lastly, the methodology of MO-FORM will be introduced and discussed. The strength of the method will be analyzed and demonstrated for a general example. MO-FORM will then be applied to a statically indeterminate truss subjected to cyclic loading.

1.4 FIGURES

Figure 1.1. FORM and SORM approximations for a component reliability analysis (Der Kiureghian 2005)

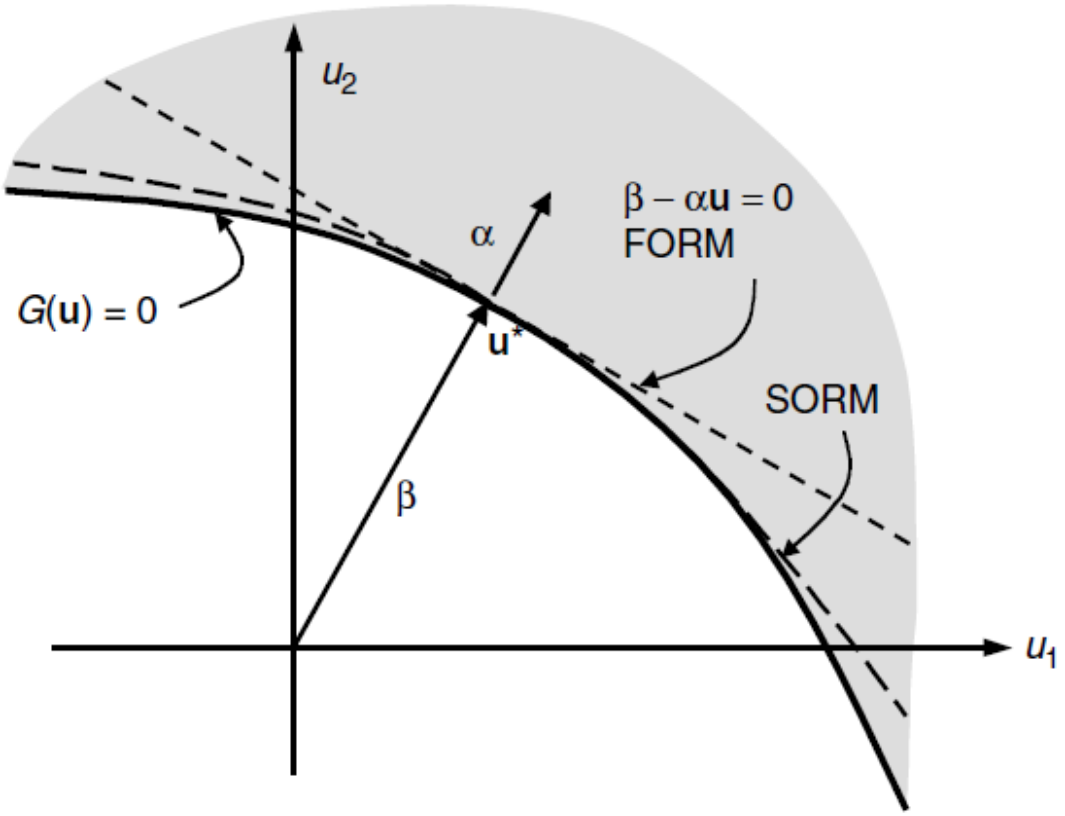

Figure 1.2. Three failure modes in the two-dimensional standard normal space (Kim 2009)

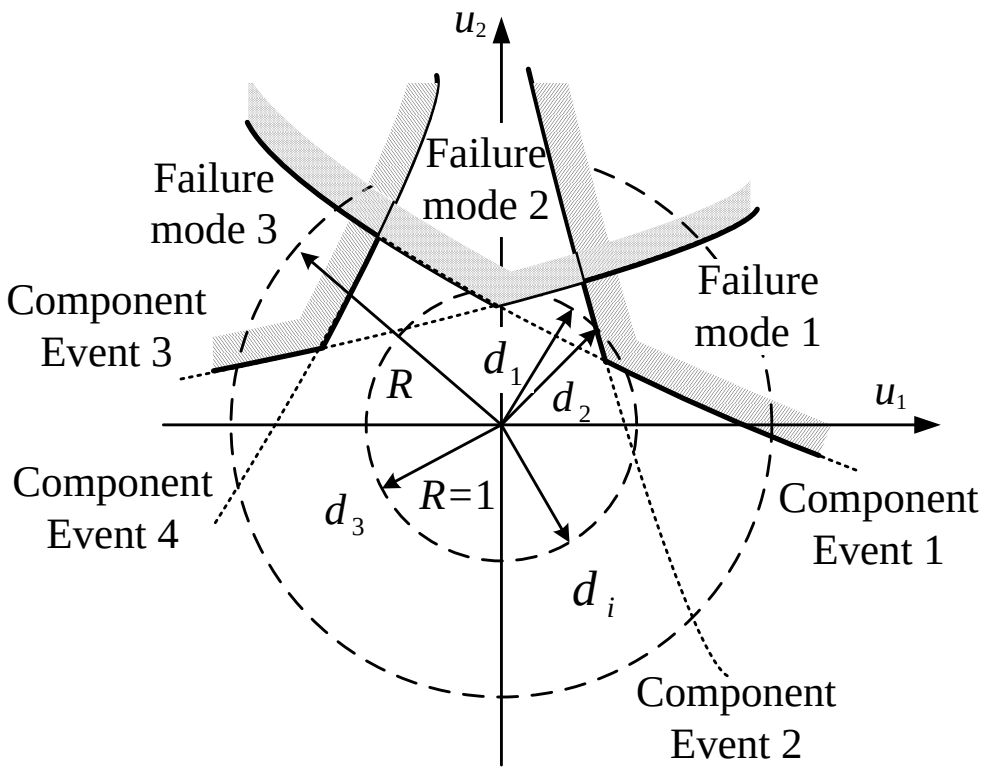

CHAPTER 2

SYSTEM RELIABILITY ANALYSIS OF FATIGUE INDUCED SEQUENTIAL FAILURES USING SELECTIVE SEARCHING ALGORITHM

2.1 BACKGROUND

Most methods developed to identify structural system failure modes can be categorized into two types of approaches (Shao & Murotsu 1999): the *probabilistic approach*, which includes the simulation based techniques (Grimmelt & Schueller 1982; Rashedi 1983; Melchers 1994) and the branch and bound method (Murotsu et al. 1984; Thoft-Christensen & Murotsu 1986; Karamchandani 1987); and the *deterministic approach*, which includes the β-unzipping approach (Thoft-Christensen & Murotsu 1986), the methods employing heuristic techniques (Xiao & Mahadevan 1994; Shetty 1994), the incremental loading method (Moses & Stahl 1978; Moses 1982; Lee 1989), or the methods based on mathematical programming (Corotis & Nafday 1989).

Generally, the probabilistic approach is considered theoretically rigorous but computationally costly, whereas the deterministic approach is computationally efficient but has risks of overlooking important failure modes (Shao & Murotsu 1999). To address these problems, Shao & Murotsu (1999) proposed an improved simulation-based selective searching technique based off of genetic algorithms (GA) (Holland 1975; Goldberg 1989) finds the few most dominant failure modes that contribute most to the system failure probability. Since GA uses a population of multiple searching points, Kim (2009) extended the approach to find multiple failure modes simultaneously. This proposed searching method differs by the one proposed by Shao & Murotsu (1999) by the two most distinct GA strategies: *searching direction* and *elitism,* as explained in the following paragraphs.

2.2 METHODOLOGY

Consider an *n*-dimensional random variable space **x** that represents all possible realizations of uncertain quantities in a system reliability problem. Using the nonlinear transformation $\mathbf{u} = \mathbf{T}(\mathbf{x})$ as discussed in Section 1.2.2 one can find a realization of the random

vector **X** in the space of standard normal random variables **u**. This **u** space can be viewed in Figure 1.2. In the figure, the dotted lines show component limit states while solid lines represent the boundaries of the failure modes which consist of multiple component limit states. Since the joint PDF in the **u** space is solely determined the distance from the origin, $\|\mathbf{u}\|$, failure modes closest to the origin are likely to make significant contribution to the system failure probability; however, it must be noted that the volume of the failure mode also affects the contribution to the system failure probability. The original method by Shao & Murotsu (1999) searches the random variable space from points on hyperspheres, starting with a larger radius, toward the origin, by generating sets of samples in the **u** space. This "inward" searching strategy is able to identify the most dominant failure modes closest to the origin. The corresponding values in the original random variable space can then be found through the inverse transform $\mathbf{x} = \mathbf{T}^{-1}(\mathbf{u})$ as described in a previous section. Each sample of **x**, or chromosome, is then ranked on its fitness function value based on its distance from the origin. The chromosomes with highest fitness function values are then selected as elite chromosomes for use in the mating pool to create the offspring for the next generation. This process is repeated until the failure mode nearest the origin is not renewed for a prescribed number of successive generations.

On the other hand, the searching method proposed by Kim (2009) reverses this search direction. This "outward" search finds multiple dominant failure modes in decreasing order of likelihood until the newly identified modes have negligible likelihoods. After this, the system failure probability can be obtained accurately from these critical failure modes. This method is implemented as follows. First, generate random samples in the **u** space for the first generation of the selective searching method. To search outward, these samples are generated on a hypersphere of smaller radius initially. This method will then be run for larger radii. If knowledge about the system reliability index is available a priori, the range of these radii must encapsulate this expected value and address the uncertainty inherent with this knowledge. From the knowledge described previously about the joint PDF in the **u** space, samples of a hypersphere of radius *R* are generated by

$$\mathbf{u}^i(R) = R \cdot \mathbf{d}^i = R \cdot \frac{\mathbf{u}^i}{\|\mathbf{u}^i\|}, \quad i = 1, \dots, N_{pop} \tag{33}$$

where $\mathbf{d}^i = \left[d_1^i\ d_2^i \ldots d_n^i\right]^T$ is a "direction" vector, i.e. a point randomly generated on the surface of a unit-radius hypersphere, which is obtained from a normalized random vector in the **u** space $\mathbf{u}^i = \left[u_1^i\ u_2^i \ldots u_n^i\right]^T$. These direction vectors constitute the initial population for the selective searching method. There are many methods that can efficiently generate the $\mathbf{u}^i$'s. For this study, Latin Hypercube Sampling (McKay et al. 1979) is used.

Second, the sampling points $\mathbf{u}^i(R)$ are transformed back to their original space using the nonlinear transformation $\mathbf{x}^i(R) = \mathbf{T}^{-1}[\mathbf{u}^i(R)]$. For a structural system, **x** may represent randomness in the capacities and material parameters in the structural components or imposed loadings. For each $\mathbf{x}^i(R)$, structural analysis is performed to determine whether or not local failures have occurred. Should any member fail, the structural analysis is repeated with that member removed. Progressive failures can then be modeled by this framework. If system failures are found, the failure mode and corresponding sample points are recorded. These failure modes are then saved for the mating pool.

Third, a selective search is performed in the vicinity of the $\mathbf{x}^i(R)$ that caused system failures. Since one structural member is often involved in multiple failure modes, unidentified additional failure modes may be relatively close to those known in the **u** space. To find these nearby failure modes, crossover between parents in the mating pool creates offspring that will be in these nearby regions. Figure 2.1 shows the crossover operation used in this method. As shown in the figure, for each allele location, a random value between 0 and 1 is generated. If this value is greater than 0.5, Parent 1's allele data is passed to the offspring; otherwise, parent 2's allele data is passed. This multi-point crossover generates the next-generation's searching points so that they search for new failure modes in the vicinity of the parent populations. This helps to maintain diversity during the search process. One must note here that crossover will always occur in the operation, so the probability of crossover is 1. Since not all failure modes may be near the first identified failure modes, the mutation operator (see Figure 2.2) is used to search far from the current failure modes by simply inverting the sign of a given allele. Here, random values are generated again, and if the number is less than the probability of mutation, which is 0.3 in Figure 2.2, the allele's sign is inverted. As discussed in a previous section, this probability should not be high, as it will greatly increase the time cost of the method.

Last, should no new failure modes be identified for a fixed number of new generations of samples, N_{same}, the hypersphere radius will be increased by a small increment and the previously described process will be repeated. One should note that if N_{same} is too small failure modes will not be found properly, and, conversely, if N_{same} is too large the method becomes computationally costly. This process of searching and expanding the hypersphere radius continues until the failure probabilities of newly identified failure modes becomes less than a prescribed fraction of the failure mode with highest failure probability.

2.3 DISJOINT CUT-SET FORMULATION

Since the component failures in the situations presented in the paper are based off of fatigue, a proper crack growth model must be used. In this thesis, the Paris-Erdogan crack growth model (Paris & Erdogan 1963) is used, i.e.

$$\frac{da}{dN} = C(\Delta K)^m \tag{34}$$

where a represents the crack length, N is the number of load cycles, C and m are material parameters, and ΔK is the stress intensity factor range. Using Newman's approximation (Newman & Raju 1981), one can represent this stress intensity factor range as

$$\Delta K = S \cdot Y(a) \cdot \sqrt{\pi a} \tag{35}$$

where S represents the far-field stress range, and $Y(a)$ is the "geometry" function, which accounts for the geometry of the crack and the applied stress. If (35) is substituted into (34) and then integrated, one can describe the time until a truss members under cyclic loading fails as

$$T_i^0 = \frac{1}{C\nu_0(S_i^0)} \int_{a_i^0}^{a_{c_i}} \frac{1}{[Y(a)\sqrt{\pi a}]^m} da \tag{36}$$

where T_i^0 is the time until the i-th member fails first, i.e. without preceding failures of other members; ν_0 is the applied loading frequency; a_{c_i} is the i-th member's critical crack length at failure; a_i^0 is the i-th member's initial crack length when no members have failed; and S_i^0 denotes the i-th member's far-field stress range in the undamaged configuration.

For *sequential* failures stemming from local member failures, one must model the load redistributions and find the time necessary for other members to fail after previous member failures. Using inspiration from Lee & Song (2010), these times are found efficiently while accounted for stress redistribution. For example, the time for the *i*-th component to fail after the local failure sequence {1→2→…→(*i*–1)} has occurred can be found using the following recursive formula

$$T_i^{1,\dots,i-1} = \frac{1}{C\nu_0\left(S_i^{1,\dots,i-1}\right)^m}\int_{a_i^0}^{a_{c_i}} \frac{da}{\left[Y(a)\sqrt{\pi a}\right]^m} - \sum_{k=1}^{i-1}\left(\frac{S_k^{1,\dots,k-1}}{S_i^{1,\dots,i-1}}\right)^m T_k^{1,\dots,k-1} \tag{37}$$

where $S_i^{1,\dots,i-1}$ denotes the *i*-th member's far field stress range after the load re-distributions inherent in the failure sequence {1→2→…→(*i*–1)}.

For given outcomes **X** = **x** during the selective search, different component failure times are compared at each step to find the failure sequence corresponding to an outcome $\mathbf{x}^i$. For example, if T_5^0 is smaller than T_i^0, $\forall i \neq 5$, the cracking failure occurs first at component 5. Afterwards, if T_2^5 is smaller than T_j^5, $\forall j \neq 5,2$, the cracking failure sequence is updated to {5→2}. This process is repeated until the damaged structure meets certain failure criteria, as described in the following section. Once the full failure sequence is obtained, if the total of the accumulated time terms, $T_5^0 + T_2^5 + \cdots + T_n^{5,2,\dots,n-1}$, is smaller than a given inspection cycle T_{ins}, $\mathbf{x}^i$ is identified as a proper system failure case, i.e. a point inside one of the shaded failure domains in Figure 1.2; otherwise, $\mathbf{x}^i$ is not a system failure case.

For the analyses in this study, a system level failure occurs if any of the following four criteria are satisfied: (1) local instability, (2) global instability, (3) excessively large stiffness matrix condition number, and (4) excessive nodal displacement. For the first criterion, since the example structure in this thesis is a planar truss, if less than two members are attached to a non-supporting node, the structure becomes locally unstable. For the second criterion, a planar truss structure becomes globally unstable if

$$2 \cdot N_{node} - N_{member} - N_{reactionDOF} > 0 \tag{38}$$

where $N_{reactionDOF}$ is the number of reaction degrees of freedom; N_{node} is the number of nodes; and N_{member} is the number of members. For the third criterion, if the condition number of the damaged structure's stiffness matrix becomes excessively large compared to that of the original structure, the structure is considered to have a system-level failure. For the last criterion, if any nodal displacements become excessively large, the system is said to have failed, since the analysis mode here is linear elastic, and such large deformations would violate these assumptions.

Using (36) and (37), a failure sequence can be described in terms of the individual component failure times. The event that describes such a system failure event, e.g. {1→2→…→(i-1)}, is (Lee & Song 2010)

$$\left[\cap_{\forall j\neq 1}(T_1^0 < T_j^0)\right] \cap \left[\cap_{\forall k\neq 1,2}(T_2^1 < T_k^1)\right] \cap \ldots$$

$$\cap \left[\cap_{\forall l\neq 1,\ldots,i}(T_i^{1,\ldots,(i-1)} < T_l^{1,\ldots,(i-1)})\right] \cap (T_1^0 + T_2^1 + \cdots + T_i^{1,\ldots,(i-1)} < T_{ins}) \quad (39)$$

The events in the first few brackets describe the component failure occurrence in the above stated failure event, such as "1 fails first," "2 fails next," until "i-th member fails last," whereas the last event indicated that the failure event occurs within the inspection cycle time. Since these failure modes are defined using a mutually exclusive cut-set formulation, the lower-bound on the system failure probability can be found by a simple addition of the failure modes identified by the selective searching technique,

$$P(E_{sys}) = \sum_{k=1}^{N_{cut}} P(C_k) \geq \sum_{k=1}^{N_{cut}^{id}} P(C_k) \quad (40)$$

where N_{cut}^{id} denotes the number of identified critical failure sequences. Since these failure sequences are mutually exclusive using (39), the statistical dependence between failure modes is fully accounted for. Lee & Song (2010) computed the probability of each failure mode, $P(C_k), k = 1, \ldots, N_{cut}^{id}$, by performing SORM for the last event in (39) and FORM for all other events, followed by an efficient sampling method (Genz 1992) to perform the system reliability analysis. For numerical examples in this thesis, due to high nonlinearity of the limit state functions in (36) and (37), FORM and SORM analyses could not obtain accurate estimates of the component event probabilities in (39). To overcome this issue, crude-MCS is used to obtain

accurate probability estimates for the identified cut-sets, replacing component analyses followed by a system reliability analysis. These probability estimates are then added in (40) to obtain the lower bound of the system failure probability; However, having to perform a separate crude-MCS to obtain failure mode probabilities does not make the current formulation of this method especially efficient when compared to general crude-MCS to obtain the system failure probability. Since this method does identify dominant failure modes and points within the associated failure domains, a method may be developed to address this issue using importance sampling in the future.

2.4 NUMERICAL EXAMPLE

The above selective searching technique is now demonstrated using a planar truss bridge structure numerical example as shown in Figure 2.3. This structure has 97 elements (E1,…,E97) and 50 nodes (N1,…,N50). At N2 and N50, there are pin connections and roller connections at N1 and N49. This structure is both internally and externally statically indeterminate to the third degree. This model was inspired by the original model of the Grand Sung-Soo bridge in Seoul, South Korea before the catastrophic failure and has the same member geometry as defined in KSCE (1995). This example differs from the original example by an addition of three members at the hinges that connect the two anchor trusses to the suspended truss to add complexity.

Various models were considered for the loadings in this example, from using field data measurements to fully theoretical simulations. Since no proper field strain data were available from the original bridge, such a data-based method used in Zhou (2006) was deemed inappropriate, in favor of using the fatigue analysis recommended by the LRFD Bridge Specifications (AASHTO 2004). This entails executing a full influence-line load analysis using a truck that weight 75% of the AASHTO design truck. This method was used since it is commonly used among structural engineers and seems to be a nice medium between field data and something fully theoretical. Once component stress values for a given damage state and for each position of the design truck are obtained, the maximum and minimum stress values are used to describe component stress ranges for use in the disjoint cut-set formulation in Section 2.3. If no stresses for a given member are large enough to initiate crack growth occur, the corresponding member's limit state can be neglected for that damage state. Using a full influence-line load

analysis is far superior than simply applying a given cyclic distributed load, since it is much more appropriate for modeling actual traffic fatigue.

See Table 2.1 for the distribution types and statistical parameters of the random variables used in this study: material parameters of the Paris-Erdogan crack growth model, i.e. C_i (mm/cycle/(MPa·mm)^m) and m_i, the initial crack lengths a_i^0 of the truss members i = 1,…,97, and the stress range multiplier I, to model the random traffic loading. Each of these random variables is modeled based on the suggestions in the literature (Lee & Song 2010). Another important aspect of these random variables is their statistical correlations. While a_i^0 are correlated amongst themselves and I is considered uncorrelated with the other random variables, C and m have been found to have very strong negative correlations in the literature, $\rho_{C_i m_i} \cong -0.97$ (Borrego et al 2001; Yarema 1982). Due to this, when the random variables must be transformed from the real space to the **u** space, i.e. **u** = **T**(**x**), C and m cannot be modeled as Nataf variables generally; however, Gardoni et al. (2002) have suggested using a linear relationship for random variables that have strong correlation, e.g. $0.7 \leq |\rho_{X_i X_j}|$, based off of known statistical parameters:

$$x_i = \mu_{X_i} + \rho_{X_i X_j} \frac{\sigma_{X_i}}{\sigma_{X_j}} (x_j - \mu_{X_j}) \tag{41}$$

where μ_{X_i} and σ_{X_i} are the mean and standard deviation of X_i. This relationship is implemented to model m as a linear function of C, decreasing the space of random variables by a third and enabling the modeling all random variables other than m as Nataf distributed for the nonlinear transformation **u** = **T**(**x**). All members are assumed to have an elastic modulus of 200 GPa. The average daily truck (ADTT) for the Grand Sung-Soo was 4,483 (Cho et al. 2000). The ADTT was multiplied by 365 days to determine the annual loading frequency v_0.

A total of 60 significant failure modes were identified by the selective searching method, whose reliability indices range from 2.9986 to 4.7534. It is also noted that 45 modes with higher likelihood have similar reliability indices between 2.9986 and 4. See Table 2.2 for a list of the seven most significant failure modes and the associated reliability indices. The existence of these many critical failure modes with similar likelihood is indicative of the high degree of symmetry and redundancy of the bridge. It should also be noted that all of these 45 most critical modes

originate at members 61, 62, 63 and 64, which are the diagonals in the center of the suspended truss. The nature of these "competing" failure modes made it necessary to identify 63 modes.

An N_{same} of 5 was used during the selective search. Using (40), the lower bound on the system failure probability with 60 modes is 2.0079×10^{-2} (generalized reliability index 2.0521). This result is verified by crude-MCS which produces a system reliability index of 2.0140 with a coefficient of variation of 6.25%. The relative error between these two methods is only 0.16%. See Table 2.3 for a list of CPU time costs for the proposed method and crude-MCS. One must note here that the selective searching method not only finds the system failure probability but also all significant failure modes; by comparison, the current formulation of crude-MCS only tallies system failures and does not keep track of the failure mode contributions. Crude-MCS can keep track of the failure mode contributions, but this would increase the computational cost of the method significantly, since for every sample generated the failure mode would also have to be saved. Since the selective searching algorithm only identifies the most critical failure modes, this coupling of failure mode identification and probability calculation in crude-MCS would show the benefit of the selective searching algorithm. One should also note that the selective searching algorithm itself only requires 441 seconds.

The selective searching algorithm has many applications for field practitioners. Using the selective searching algorithm for a given inspection cycle time, one can find the critical members that are the root of cascading fatigue induced failures and devote more attention to controlling damage and implementing repairs for these members. One can also find the most likely failure paths and be sure to stop cascading failures should component failures occur.

2.5 FIGURES

Figure 2.1. Crossover genetic operator for selective searching method (Kim 2009)

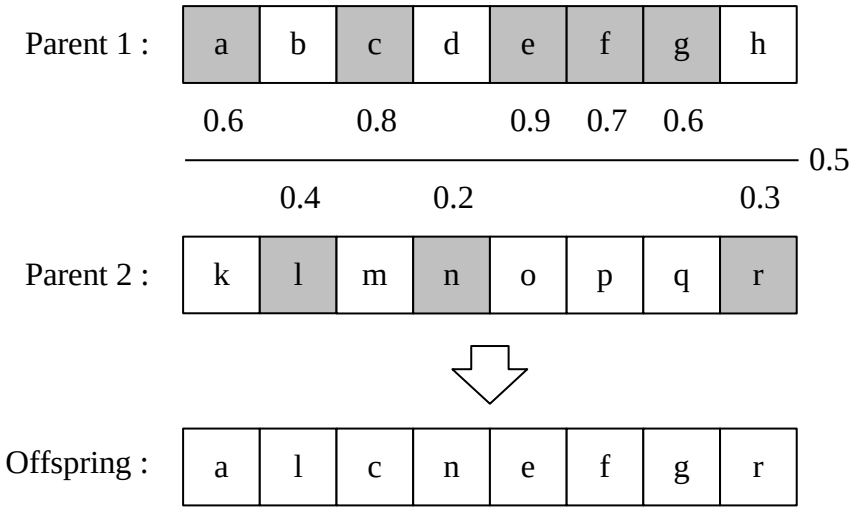

Figure 2.2. Mutation genetic operator for selective searching method (Kim 2009)

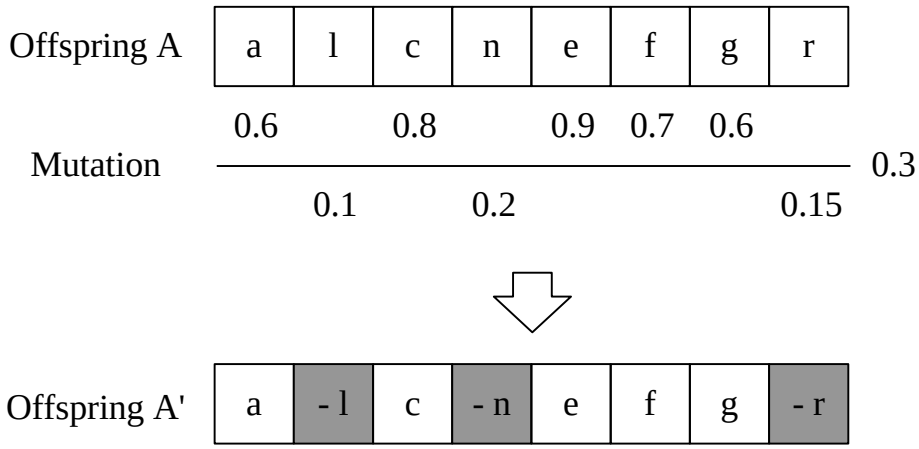

Figure 2.3. Planar truss bridge example

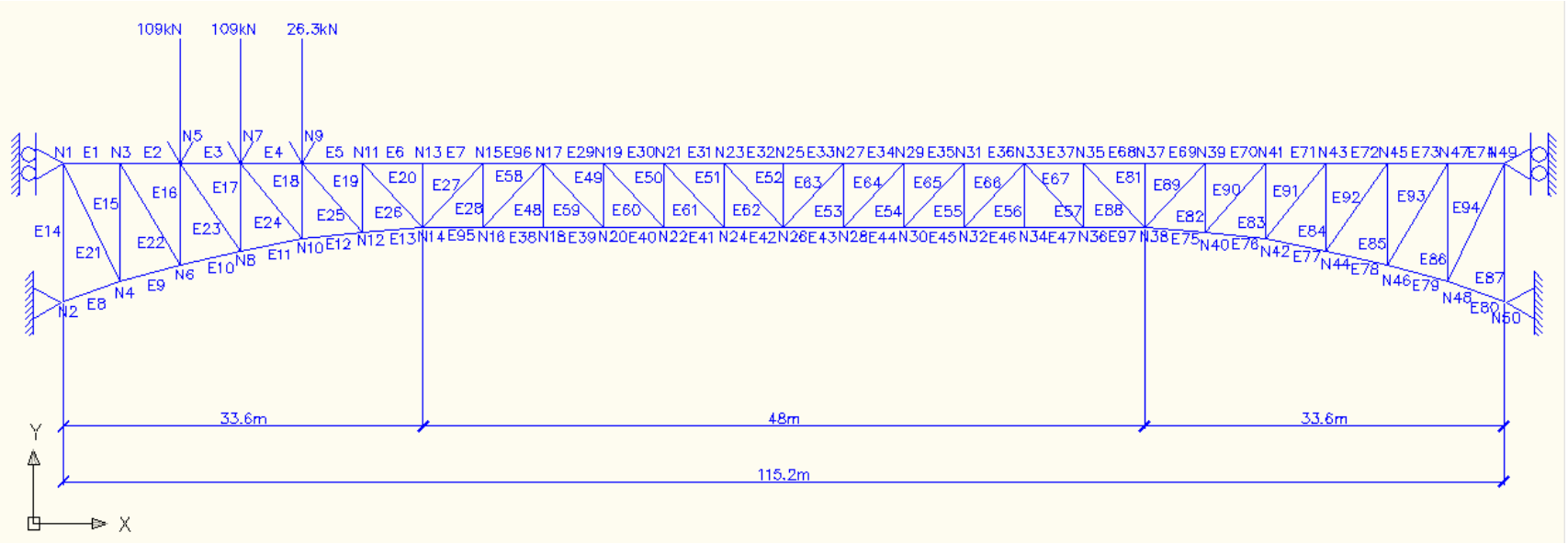

2.6 TABLES

Table 2.1. Distribution types and statistical parameters of random variables

Random variable	**Distribution**	**Mean**	**Coefficient of Variation**
C	Lognormal	$1.202 \cdot 10^{-13}$	0.533
M	Lognormal	3	0.02
a^0	Exponential	0.11 mm	1
I	Normal	1	0.1

Table 2.2. Reliability indices of seven dominant failure sequences.

Failure Sequence	**Reliability Index**
61→64	2.9986
64→61	3.0193
62→64	3.1159
63→61	3.1389
61→63	3.1523
61→68→6	3.1701
61→68→7	3.1728

Table 2.3. Computational cost for the proposed method and MCS

	CPU time (seconds)
Proposed Method	Failure mode search time: 441.0 sec (7.35 min) **Total time: 26,992 sec (7.50 hrs)**
Crude-MCS	**Total time: 27,024 sec (7.51 hrs)**

CHAPTER 3

MULTI-OBJECTIVE FIRST-ORDER RELIABILITY METHOD

3.1 BACKGROUND

As described in Section 2.3, the critical term in (39) of the disjoint cut-set formulation is determined by the inspection cycle T_{ins}, a time usually unknown a priori and based off of precedence and not proper risk informed decision making. To help field practitioners make better decisions, a multi-objective genetic algorithm is hereby proposed to find the reliability indices of many inspection cycle times at once, which is termed as multi objective first order reliability method (MO-FORM). This method is not hindered by local solutions as gradient-based design point search methods are, and does not have issues finding events that are highly unlikely (high reliability index) but possible critical failures, as they occur for small inspection cycle times, unlike crude MCS. The two objectives functions in this situation are the reliability indices and inspection cycle times. For this example, genetic algorithm-based search was chosen among many candidate algorithms for multi objective optimization. Due to its ease of implementation and fast convergence, the Non-dominated based Sorting Genetic Algorithm II (NSGA-II) (Deb et al. 2002) was selected in particular. NSGA-II is a modified version of the original NSGA that incorporates elitism and does not require an a priori sharing parameter. This multi-objective method obtains a surface of non-dominated solutions, so-called Pareto surface.

3.2 METHODOLOGY

Several concepts regarding multi objective optimization must be explained before presenting the details of the proposed method. NSGA-II executes as follows: (1) initialize the population, (2) obtain objective function values, (3) assign fitness function values based off of Pareto Optimality, (4) find crowding distances, (5) find elite chromosomes for the mating pool, (6) use the genetic operators of mutation and crossover to obtain the new population, and (7) repeat the process until the result converges. Each of these will be discussed in the section to follow. Before beginning this discussion, NSGA-II requires two important parameters: N_{pop}, the fixed number of chromosomes in each population, and N_{gen}, is the required number of generations.

First, initialize the population. This can be achieved in many ways as described in Section 2.2 for the selective searching method. Many different options were investigated over the course of this study, but the final method selected used LHS in the **u** space and then normalized each sample. These samples were then scaled so that their magnitude was much smaller than one. These magnitudes are equivalent to the reliability indices. Depending inversely on the number of random variables, these magnitudes could be anywhere between the order of 10^{-2} and 10^{-10}. An issue with this method is its need for pre-specified bounds on each random variable during the evolution process. Due to the nature of the a_i^0 being correlated random exponential variables, if one imposed these boundaries in the **u** space, when they are transformed back to the original space, some margins may become zero and infinity, causing this method to fail. This is a result of the scale of the problem as well as the correlations between random variables. These margins are used to fix the range of the values of the random variables so that crossover and mutation do not create offspring that consistently prevent proper convergence of NSGA-II. Initially they were used to sample the first population from a shifted uniform distribution as well as impose boundaries on the offspring. To remedy these issues, tight sampling around small reliability index values in the **u** space was used. The successive generations quickly populate a pre-specified range of reliability indices despite these issues.

Second, obtain values of the objective functions. The first objective function is the reliability index. This is simply the magnitude of the sample in the **u** space and reciprocally corresponds to the likelihood of a failure event. The second objective function is the amount of time it takes for the system to fail based off the criteria discussed in Section 2.3. Since the failure modes are calculated using the disjoint cut-set formulation, the times between component failures can simply be calculated using (36) and (37) and summed to find the time until failure. These total failure times can then be considered to be the inspection cycle time threshold value for a given likelihood, since that would correspond to a system failure for the limit state

$$g(\mathbf{x}) = \sum_{i=1}^{n} T_i^{1,\dots,i-1} - T_{ins} \leq 0 \tag{42}$$

where the first term on the right-hand-side of the equation represents the "performance function." The performance function is simply a measure of criticality. The higher the threshold value, the less critical the event. Thinking of this performance function as the length of time until failure,

larger values are less critical, since the structure will have a long period of time before the particular failure sequence occurs. If this value is small, then it is very critical because not much time will pass until the structure will fail, which leaves little time for inspection and maintenance actions. A graphical representation of these two objective functions and the resulting Pareto Surface is shown in Figure 3.1. One should also know that this performance function is a general concept. Any type of limit state that has a form similar to (42) is generally applicable to this kind on interpretation, i.e. yielding in a structural member ($g(\mathbf{x}) = \sigma_{component} - \sigma_y \leq 0$). If the stress in a member is beyond that of the yield strength of the member, the member is said to have failed. The member may also have a range of possible yield strengths due to different types of materials.

Third, assign fitness function values based off of Pareto Optimality. Pareto Optimality is a general condition that occurs when no "Pareto Improvements" exist. A Pareto Improvement is a condition defined as a change in allocation of some quantity for a random variable where that variable is "improved" and no other variable becomes "worse off." A feasible solution **x*** is a non-dominated or Pareto optimum if and only if there exist no feasible vector **x** where

$$f_m(\mathbf{x}) \leq f_m(\mathbf{x}^*) \text{ for all } m \in \{1, \dots, n\} \tag{43}$$

$$f_m(\mathbf{x}) < f_m(\mathbf{x}^*) \text{ for at least one } m \in \{1, \dots, n\} \tag{44}$$

where *n* is the number of objective functions. For a graphical explanation of this, see Figure 3.2. Here the feasible domain is up and to the right and depends on the problem definition and specifics. The Pareto surface are the points where there are no other possible points for smaller values of either objective function, $f_1(\mathbf{x})$ or $f_2(\mathbf{x})$. For the situation in this paper, these two functions are the reliability index and the time until the system failure respectively as discussed earlier. The fitness function value for NSGA-II uses these definitions of Pareto Optimality to sort chromosomes into "fronts." Each front is based off of whether or not a chromosome is "dominated" (or has higher objective function values) than another chromosome. If not, this chromosome is considered to be non-dominated and placed in front number one. Based off of how dominated each chromosome is, they will be sorted to other fronts until all chromosomes

have been assigned a front value. To iterate, these fronts correspond to the objective function values.

Fourth, find "crowding distances" between chromosomes. Since the fitness function here is discrete based on which fronts chromosomes are in, many chromosomes will have the same fitness function values, making it necessary to have an additional parameter, crowding distance, to determine if a chromosome is a more ideal member for the mating pool. The crowding distance parameter is a measure of how densely points are distributed on a given front and is calculated by the average difference between the chromosomes that have the objective function values immediately lower and higher than the given chromosome, i.e.

$$c_{ji} = \frac{f_i(x_{j+1}) - f_i(x_{j-1})}{f_i(x_n) - f_i(x_1)} \tag{45}$$

where c_{ji} is the crowding distance for the i-th objective function, where $i = 1, \dots, m$, of the j-th chromosome, where $j = 1, \dots, n$. For the chromosomes with the highest and lowest objective functions on a front, since there are not chromosomes on either side, c_{ij} is infinite. This process is repeated for each objective function. Once completed, the overall crowding distance for a given chromosome is obtained by

$$c_j = \sum_{i=1}^{m} c_{ji} \tag{46}$$

Since MO-FORM finds a surface of Pareto optimal points, having points spaced as far as possible from each other is desirable, making larger c_j more desirable and their corresponding chromosomes elite.

Fifth, populate the mating pool with elite chromosomes. Now that the crowding distances and fitness function values are known, the mating pool can be populated. To obtain the mating pool, a tournament selection process is used. Tournament selection requires two parameters: "pool size" and "tour size." The pool size is the number of parent chromosomes in the mating pool. This is typically half the population size (Deb et al. 2002). The tour size is the number of chromosomes compared at a given time for a spot in the mating pool. This is typically two. Despite the idea that a higher tour size would cause more diversity in selection and perhaps

better convergence, higher tour size values seem to have little effect. For a given tour, chromosomes are given priority for a higher fitness function value, e.g. the lowest front, and, if chromosomes are on the same front, larger crowding distance to encourage even spreads over the Pareto optimal surface. This process of generating tours continues until the mating pool is fully populated. Now that mating pool has been selected, the offspring population can be created using genetic operators.

Sixth, use the genetic operators of mutation and crossover to obtain the new population as described in Deb & Agarwal (1995). Simulated binary crossover is used for this method. This method is also a multi-point crossover operator, like the crossover operation described in Section 2.2, and is described below:

$$c_{1,j} = \frac{1}{2}[(1 - \vartheta_j)p_{1,j} + (1 + \vartheta_j)p_{2,j}] \tag{47}$$

$$c_{2,j} = \frac{1}{2}[(1 + \vartheta_j)p_{1,j} + (1 - \vartheta_j)p_{2,j}] \tag{48}$$

where $c_{i,j}$ is the i^{th} child with j^{th} component, $p_{i,j}$ is the i^{th} parent with corresponding j^{th} component, and ϑ_j is a number sampled from probability density

$$p(\beta) = \frac{1}{2}(\eta_c + 1)\vartheta^{\eta_c}, \text{ if } 0 \leq \vartheta \leq 1 \tag{49}$$

$$p(\beta) = \frac{1}{2}(\eta_c + 1)\frac{1}{\vartheta^{\eta_c+2}}, \text{ if } 1 < \vartheta \tag{50}$$

where η_c is the distribution index for crossover. This is a value defined a priori, which is used as 20 in this situation. The above relationships are then used to find

$$\beta(u) = (2u)^{\frac{1}{\eta_c+1}}, \text{ if } 0 \leq \vartheta \leq 1 \tag{51}$$

$$\beta(u) = \frac{1}{(2(1-u))^{\frac{1}{\eta_c+1}}}, \text{ if } 1 < \vartheta \tag{52}$$

where u is a uniformly sampled random variable between (0,1). Crossover is implemented in this method with a 90% crossover rate. If crossover does not occur, mutation is used. In this method, polynomial mutation is used. To obtain an allele of the child chromosome $c_{i,j}$, use

$$c_{i,j} = p_{i,j} + \left(p_{i,j}^{u} - p_{i,j}^{l}\right)\delta_j \tag{53}$$

where $p_{i,j}^{u}$ being the upper bound and $p_{i,j}^{l}$ being the lower bound on a given parent component, and δ_j is found from the polynomial distribution as follows:

$$\delta_j = \left(2r_j\right)^{\frac{1}{\eta_m+1}} - 1, \text{if } r_j < 0.5 \tag{54}$$

$$\delta_j = 1 - \left[2\left(1 - r_j\right)\right]^{\frac{1}{\eta_m+1}}, \text{if } r_j \geq 0.5 \tag{55}$$

where r_j is a uniformly sampled random variable between (0,1) like u, and η_m is a mutation distribution index, similar to η_c, defined as 20 in this situation. Now that the offspring have been found, leeching is performed with respect to the parent population. This is done simply by taking both populations, sorting them by front and crowding distance as a whole, and then taking the resulting sorted population with the lowest front values and largest crowding distances as the next population. This seven-step process is then repeated N_{gen} number of times.

3.3 MERITS OF THE MULTI-OBJECTIVE FIRST-ORDER RELIABILITY METHOD

Before implementing this method in numerical examples, several merits of MO-FORM are presented. First, unlike conventional gradient-based optimization algorithms, MO-FORM does not require gradients of the limit state functions to obtain design points. This is particularly useful when the limit state functions are highly nonlinear or discontinuous, which is a situation that may cause FORM to find an incorrect local solution or diverge. Additionally, MO-FORM has the ability to model discrete random variables, if need be. MO-FORM also finds many design points for the full structural system simultaneously, making it unnecessary to repeat FORM many times over a large range of reliability indices. This method is particularly useful when the inspection cycle time, or threshold value, is unknown, as many FORM analyses may be required to find an appropriate value. By choosing a performance function and the reliability

index as objective function, MO-FORM generates a Pareto surface. As seen in Figure 3.3, for a given value of the performance function value, one can find the most likely failure case. This case is indicated by the red arrows. The shaded red region represents all of the less likely cases. Likewise, for a given likelihood, one can find the smallest value of the performance function, as shown by the black arrows. The shaded grey region represents all of the larger values of the performance function. MO-FORM can also handle the cases of high reliability index values, or "rare but critical," well, unlike general brute-force MCS. From the resulting Pareto surface, termed as "Design Surface," one can obtain a first order approximation of probability functions, CDF and PDF, of the time until failure or whatever performance quantity is being modeled. From this approximate PDF, the statistical moments for this performance quantity can be found. Using the points on the Pareto surface, relative contributions of the random variables can be modeled, similar to the $\hat{\boldsymbol{\alpha}}$ vector described earlier. The corresponding $\hat{\boldsymbol{\gamma}}$ vector can also be found from this information to model the effects of correlations.

3.4 SIMPLE NUMERICAL EXAMPLE

First, a simple theoretical example will be analyzed by MO-FORM. Letting the performance function, g_0, be

$$g_0(\mathbf{x}) = x_1^2 - (x_2^2 + x_3^2 - x_2 x_3) \tag{43}$$

where $x_i, i = 1, \ldots, 3$ are random variables defined in Table 3.1, and g_0 corresponds to the first term in (42). The objective functions are the same as those described previously, except that the inspection cycle time has been replaced with a general, measure of criticality. Also, X_1 is statistically independent of the other random variables, and X_1 and X_2 are correlated with correlation $\rho_{X_1 X_2} = 0.3$. For 50 in a population and 500 generations, the resulting Pareto surface is shown in Figure 3.4. This plot can be interpreted as follows: for the likelihood $\beta = 1.42$, the most critical performance would be $g_0(\mathbf{x}) = 2$.

If design changes occur, this Pareto surface will be affected in many ways. If the standard deviation or mean of X_1 is changed, the Pareto surface is affected as shown in Figure 3.5. If the μ_{X_1} is increased from 250 to 300, the Pareto surface uniformly shifts outward. Since X_1 takes the

role of a "capacity" type variable in the performance function, an outward shift that makes each value of the performance function less likely by increasing the reliability index at each value is expected. If σ_{X_1} is decreased from 50 to 30, a rotation about the zero reliability index occurs. Since decreasing the variability does not directly relate to an increase of system performance at every performance level, this does not seem unreasonable. A decrease in this variability seems to give better performance for highly critical events than an increase in μ_{X_1}. If parameters in the performance functions are varied, other changes are expected, as shown in Figure 3.6. For increases on the exponents in (43), the "frequent but less-critical" range is improved, but the "rare but more critical" range is degraded. This is another case where Pareto surface rotation occurs. The most important merit of MO-FORM is its applicability to any general case. The above examples are simply possible changes that are easily modeled by MO-FORM, but are by no means exhaustive.

One should note here that these graphs only include positive values of the reliability index. While this is reasonable for most systems because most systems are not designed to have failure probabilities greater than 50%, the negative reliability index range can be obtained by either re-running MO-FORM for negative values of the of the performance value and then flipping the signs as a post-process, or by finding the performance function value that has a zero reliability index value and performing a clever rotation procedure where the Pareto surface is rotated 90° counterclockwise above this value of performance function during the algorithm and then 90° clockwise as a post-process. If this is done for the current numerical example, the result is shown in Figure 3.7. MO-FORM can model the full range of the reliability index. A MCS curve for one million samples is also plotted here for comparison. One can see that both the large negative and large positive values, e.g. the very likely but uncritical and highly unlikely but critical, of the reliability index are captured accurately at both tails by MO-FORM, while MCS cannot cover the same region nearly as well.

Since the full range of reliability index has been obtained, now the CDF and PDF can be obtained from MO-FORM. To obtain the CDF from the Pareto surface, simply use the following equation

$$F_{g_0}(g_0^*) = P(g_0(\mathbf{x}) \leq g_0^*) = \Phi[-\beta(g_o^*)] \tag{44}$$

where $\Phi[...]$ is the standard normal CDF and $F_{g_0}(g_0^*)$ is the CDF of the performance function values at g_0^*. The CDFs from both the MCS and MO-FORM for the current example are shown in Figure 3.8. The agreement for these MCS with MO-FORM is fairly strong here. From Figure 3.9, one can also see that MO-FORM encapsulates the tail behaviors for critical values of the performance function, while the MCS cannot properly cover this region without further sampling. The PDF of the Pareto surface can be also found by the following equation from basic statistics and the chain rule

$$f_{g_0}(g_0^*) = \frac{dF_{g_0}(g_0^*)}{dg_0^*} = -\varphi[-\beta(g_0^*)]\frac{d\beta(g_0^*)}{dg_0^*} \tag{45}$$

where $\varphi[...]$ is the standard normal PDF. Since numerical issues arise from evaluating $\frac{d\beta(g_0^*)}{dg_0^*}$, cubic spline curve fitting is used to obtain the PDF directly from the Pareto surface. The result of this operation with a comparison of MCS is shown in Figure 3.10. Once can see that MCS agrees strongly with MO-FORM in this picture. Now that the approximate PDF has been obtained all statistics of the performance function can be obtained approximately, e.g. $\mu_{g_0^*}, \delta_{g_0^*}$, etc. Relative measure of importance can also be found from the chromosome values that correspond to points on the Pareto surface, information that in unattainable from the MCS result. Since only three random variable are present in this example, the Pareto surface can be visualized in the space of random variables as a three dimensional line (see Figure 3.11). One can see that different random variables dominate regions in different parts of the Pareto surface from here. For example, changes in X_1 directly affect the Pareto surface for both frequent but less critical cases as well as rare but more critical cases. Figure 3.11 shows a decent modeling of relative importance measure for problems with few random variables, e.g. 2 or 3. For larger problems, a separate representation has been developed, as will be described in Section 3.5.

3.5 FULL BRIDGE NUMERICAL EXAMPLE

Now as an application of MO-FORM to a structural system, consider the truss structure shown in Figure 3.12. There are a total of 20 members in the model subjected to two applied cyclic loads at the upper corners, and a pin and roller at the base corners. This structure is externally statically determinate, while internally statically indeterminate to the fourth degree,

like many types of structures found in the field. These applied forces may be thought of as load affects from typical horizontal loads, such as wind loads. Here, the same system failure criteria and disjoint cut-set formulation are used to describe system failures as used previously. Unlike the simple previous simple example, this is a structure subject to the risk of the fatigue-induced cascading failures, and the first objective function is the time until the system failure, not just a general criticality function. For each member, the random variables described in Table 2.1 are used to describe the uncertainties in the material properties and initial crack lengths. Each member also has a modulus of elasticity of 200 GPa. Each vertical member has a sectional area of 1,000 mm^2, horizontal member a sectional area of 2,000 mm^2, and diagonal member a sectional area of 500 mm^2.

Using 500 in a population and 2,000 generations, one obtains the Pareto surface in Figure 3.13. In contrast, using 1,000 in a population and 1,000 generations, one obtains the Pareto surface in Figure 3.13. These two results of MO-FORM are compared with a surface created from brute-MCS of 10^6 samples and a surface created from a few system-level FORM analyses. One can see from these two results that even though these two MO-FORM results have the same number of overall sample points, that the result for 1,000 in a population and 1,000 generations is slightly improved. One can also see the CPU times for the two MO-FORM results and crude-MCS in Table 3.2. While crude-MCS can obtain a Pareto surface more quickly, one must also note that MCS does not find the specific values for the individual random variables on the curve or properly encapsulate the behavior in the negative reliability index region. Since NSGA-II restricts MO-FORM to only finding points in the feasible domain, one must conclude that the MCS needs further sampling to properly represent the negative region and that both the FORM and crude MCS results are dominated (see Figure 3.2) by MO-FORM. With higher sampling, MCS will converge better, but this would make MCS take a good deal longer. The sampling that MCS uses is also affected by the number of random variables used. For higher numbers of random variables, MCS requires an exceedingly large number of points to capture the surfaces in Figures 3.13 and 3.14, which makes general crude-MCS inappropriate for identifying Pareto surfaces.

Generating the CDF and PDF of the results of the MO-FORM analysis using 1,000 in a generation and 1,000 in a population in Figures 3.15 and 3.16 respectively, one can see strong

agreement from the results generated by crude-MCS. In Figure 3.17, one can see the relative importance values as found for the equivalent correlated normals, $\hat{\gamma}^2$, as described previously. Two random variables stand out the most from this figure, No. 31 and No. 41. No. 31 represents the initial crack length of the eleventh member, which is the vertical member at the bottom right area of the truss. No. 41 is the stress range multiplier to encapsulate randomness in the applied loads. While the eleventh member's initial crack length is not obvious as an important random variable, one would expect the stress range multiplier to have a large effect here, since it directly impacts the amount of time needed for local failures in every member. One must note here that Figure 3.17 cannot be obtained from crude-MCS.

MO-FORM has many possible applications for field practitioners. Particularly for better decision making related to inspection cycle times, one can use MO-FORM to find the more likely but less critical cases and the less likely but more critical cases. From this information one can find the optimal inspection cycle time to prevent the likely cases and know what critical cases to be concerned with. One can then use the proposed importance measure scheme to find which random variables contribute most to the system failure and control them through inspection and repair.

3.6 FIGURES

Figure 3.1. Two objective functions of MO-FORM and Pareto surface

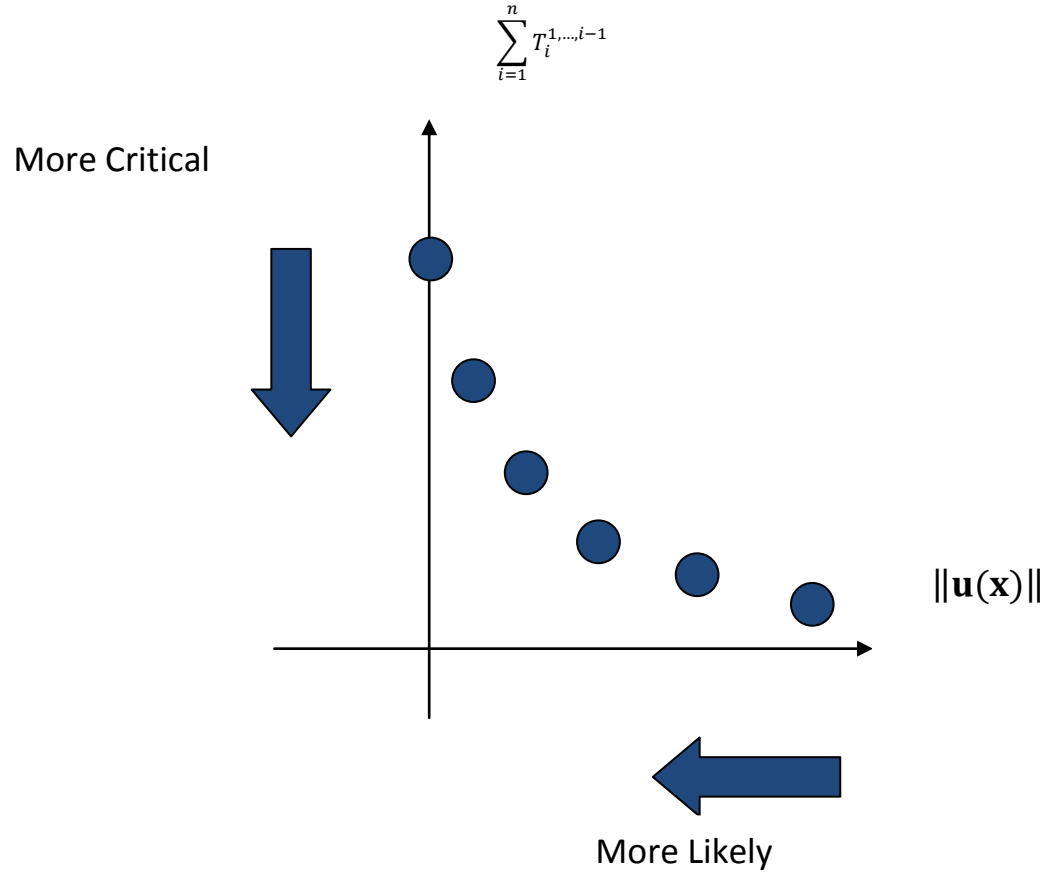

Figure 3.2. Pareto optimal (non-dominated) surface

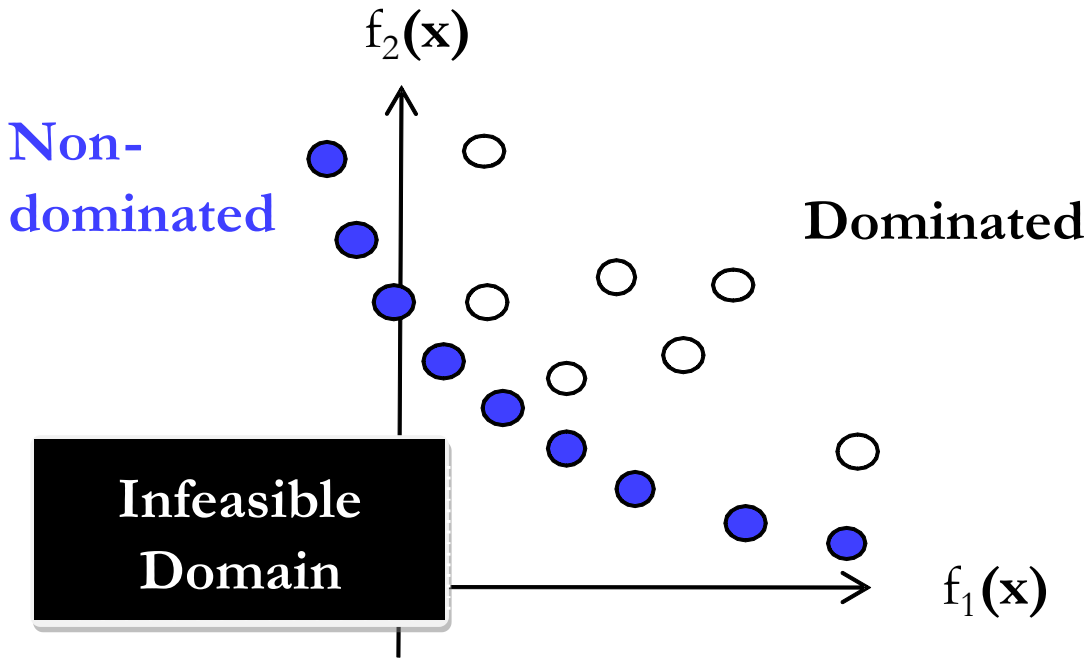

Figure 3.3. Pareto surface interpretation

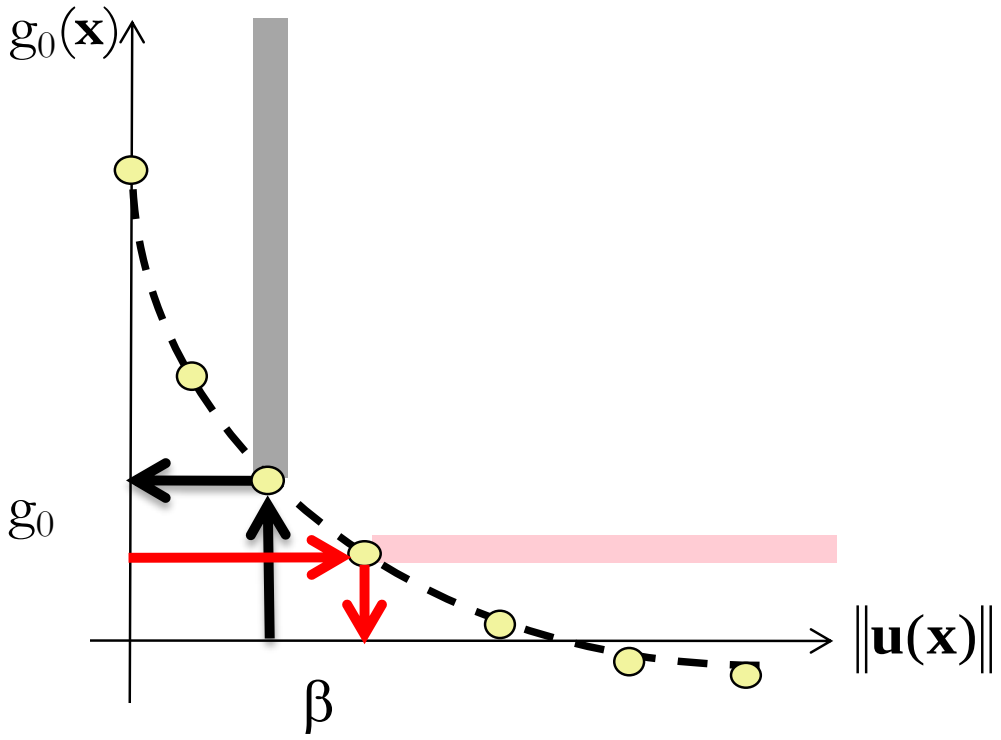

Figure 3.4. Pareto surface for the simple MO-FORM example for 50 in a population and 500 generations.

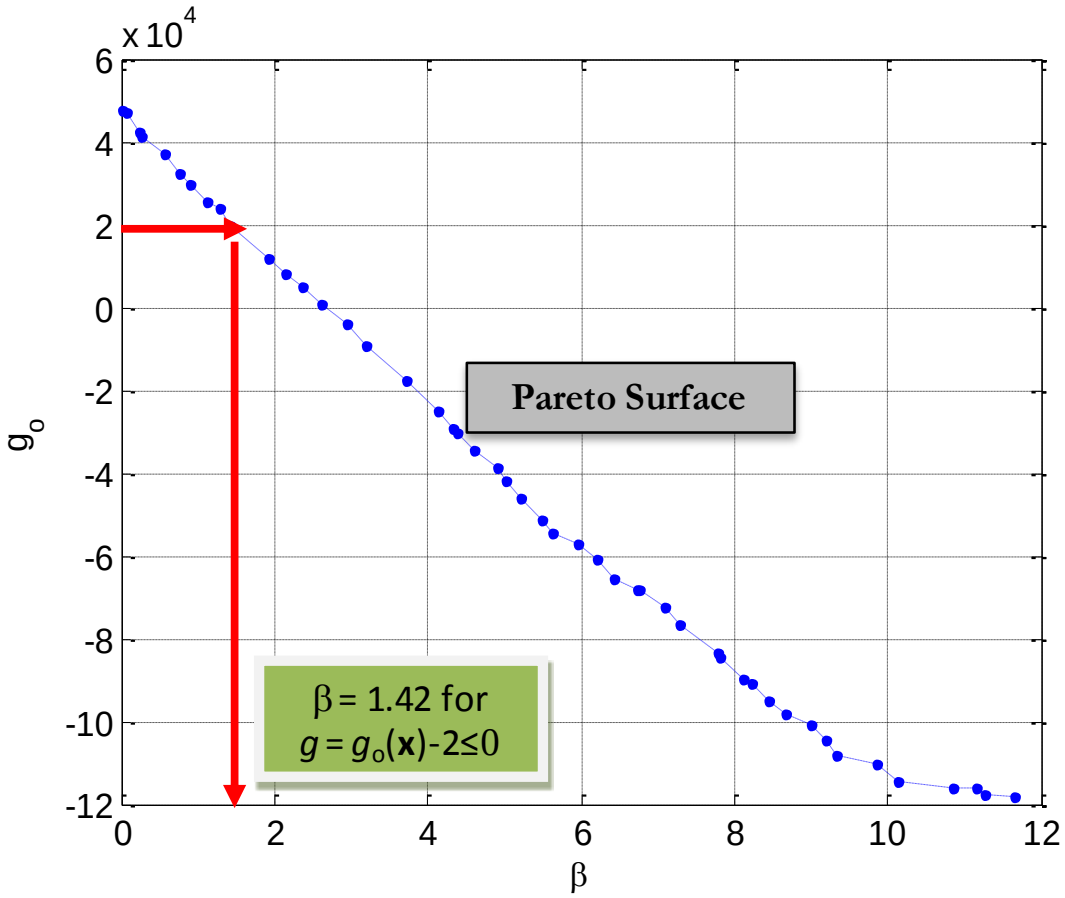

Figure 3.5: The effect of changes in X_1 statistics on the Pareto surface

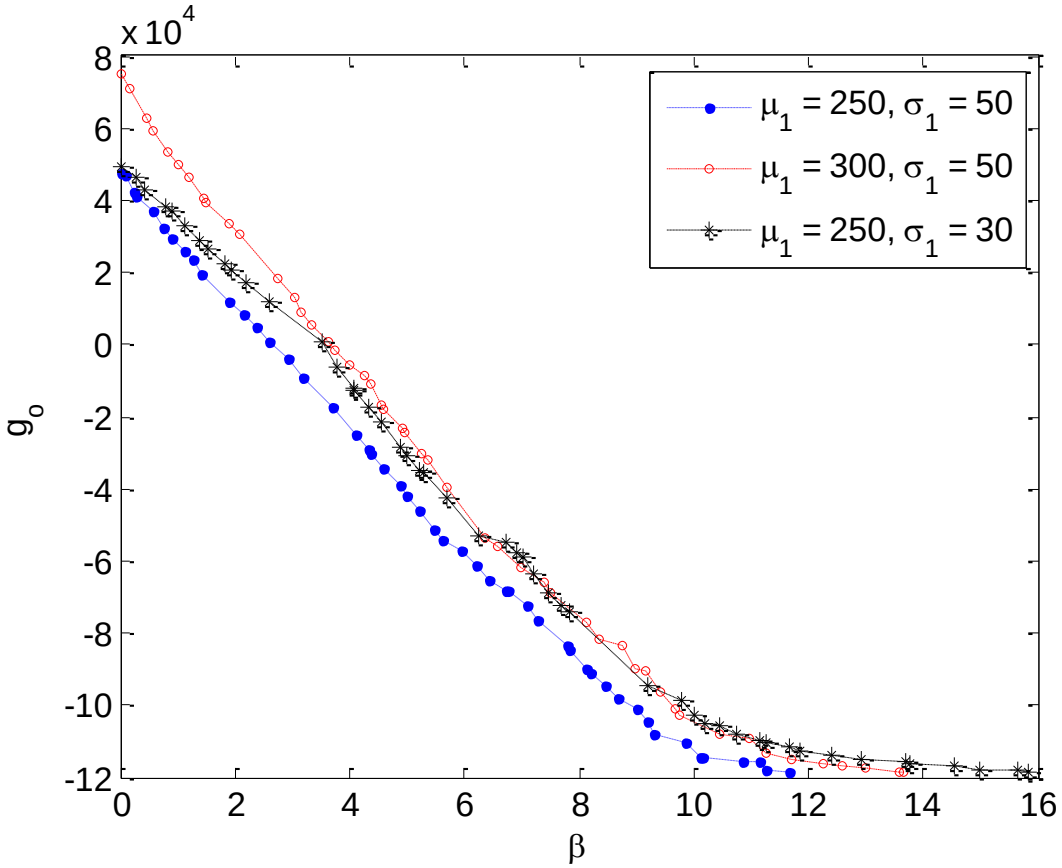

Figure 3.6: The effect of performance function parameter changes on the Pareto surface

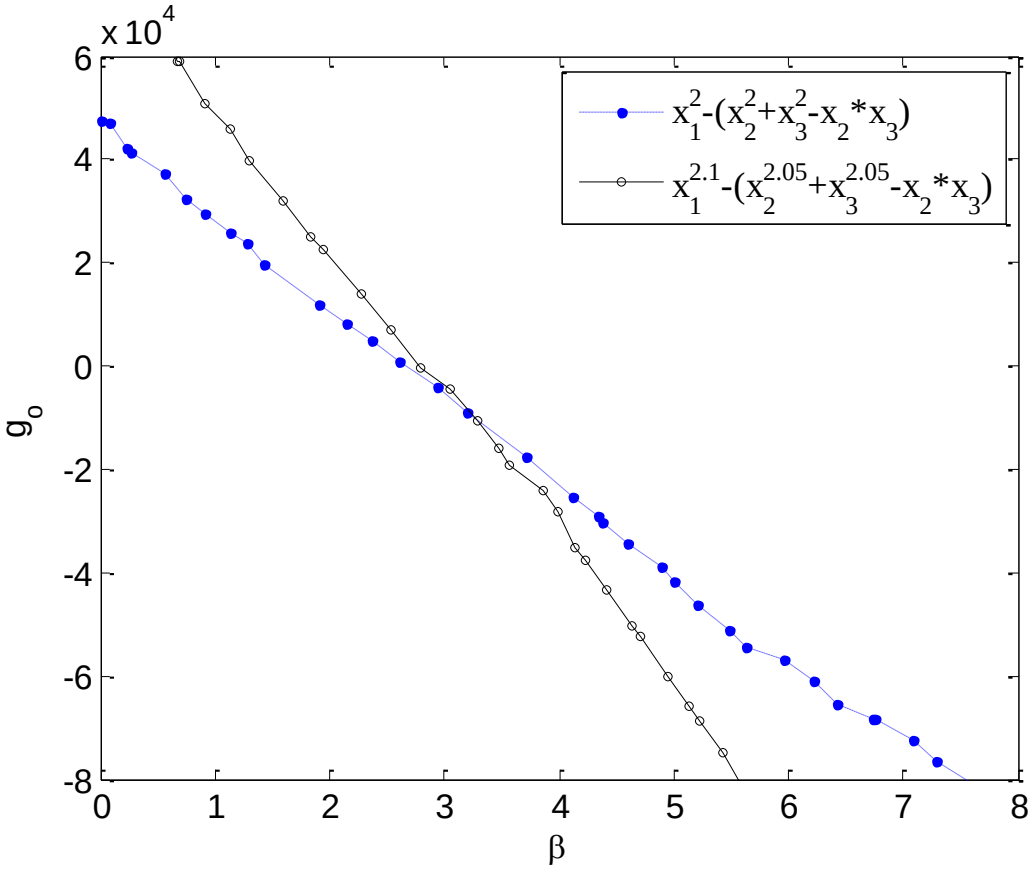

Figure 3.7: Pareto surface for the full range of reliability index

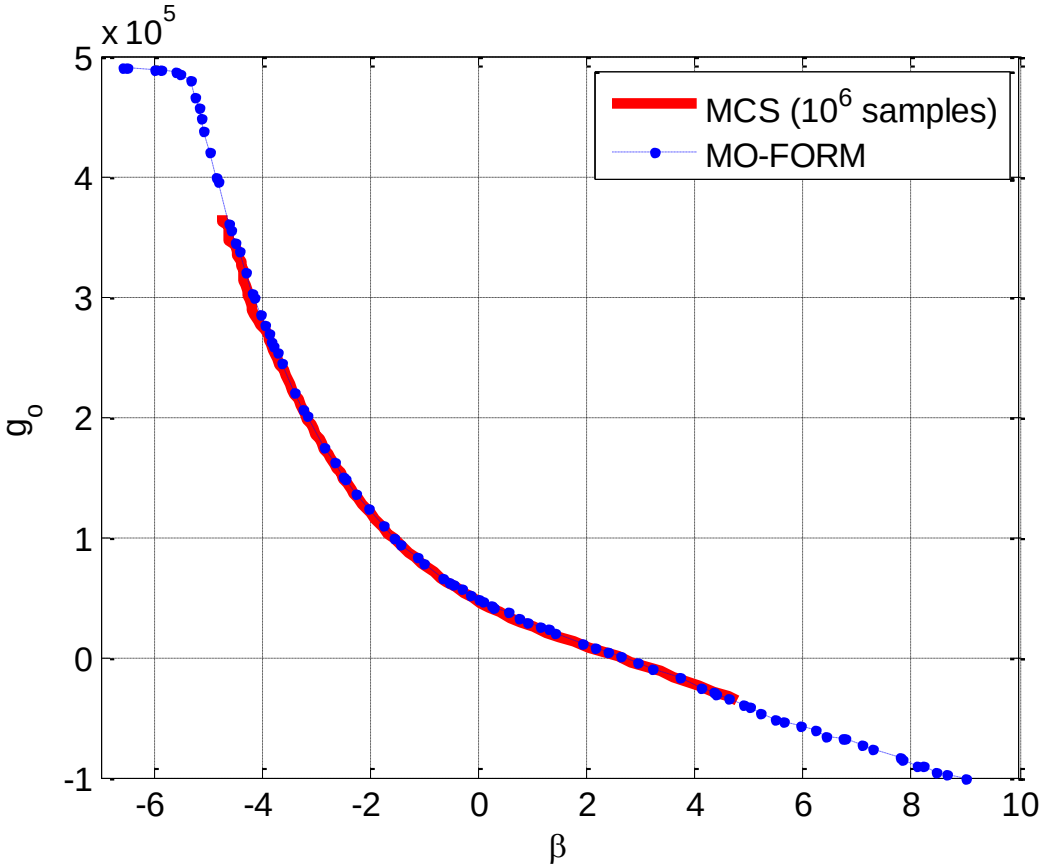

Figure 3.8: CDF of the performance function $g_0(\mathbf{x})$ by MO-FORM and MCS

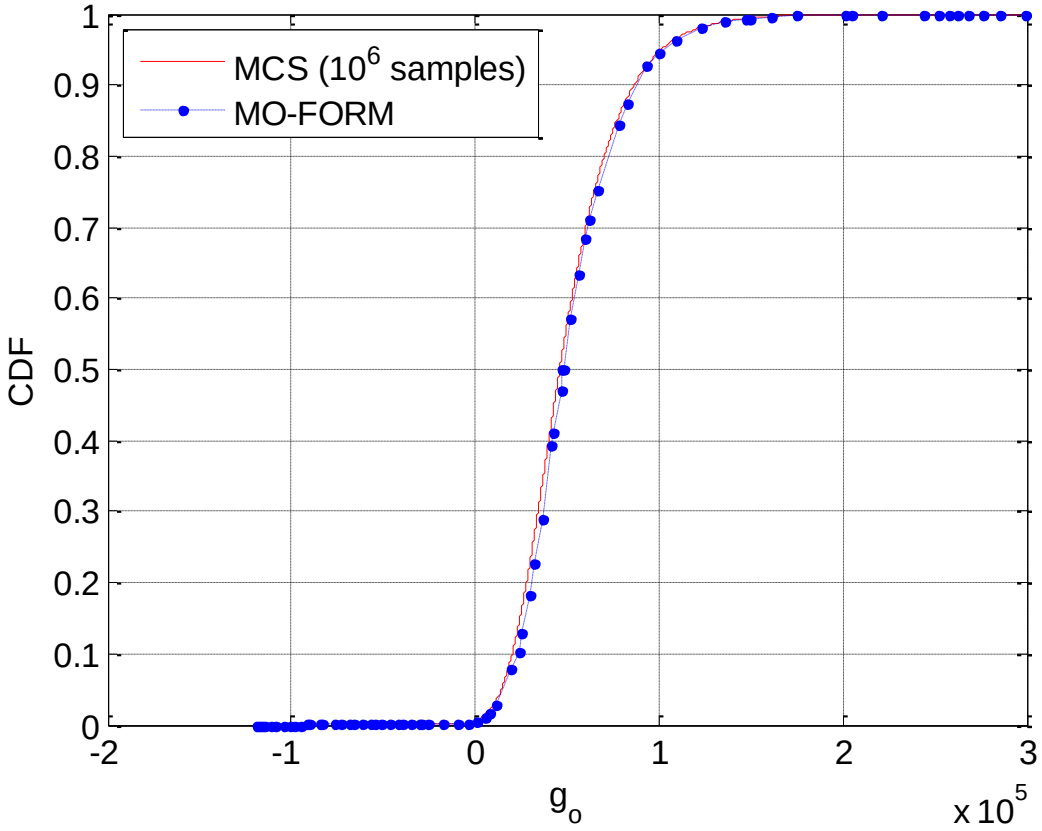

Figure 3.9: Tail behaviors of CDFs obtained by MO-FORM and MCS

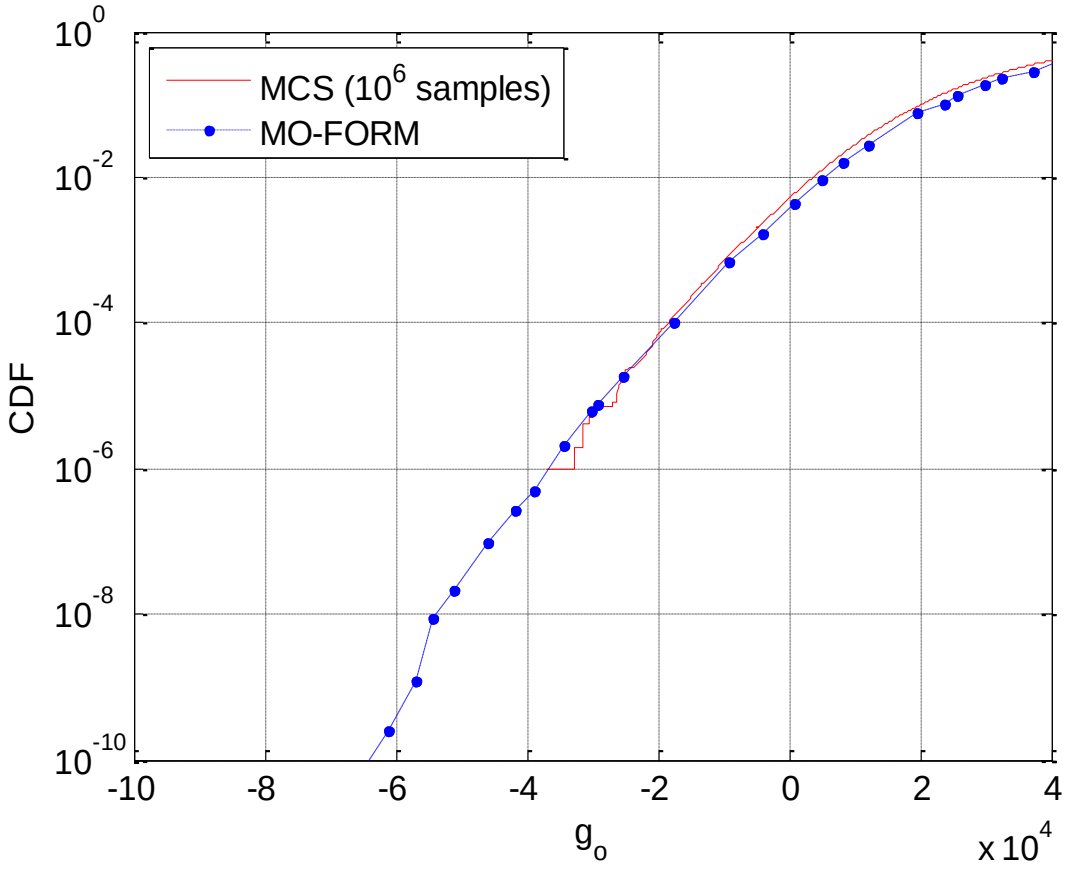

Figure 3.10: PDF of the performance function obtained by MO-FORM and MCS

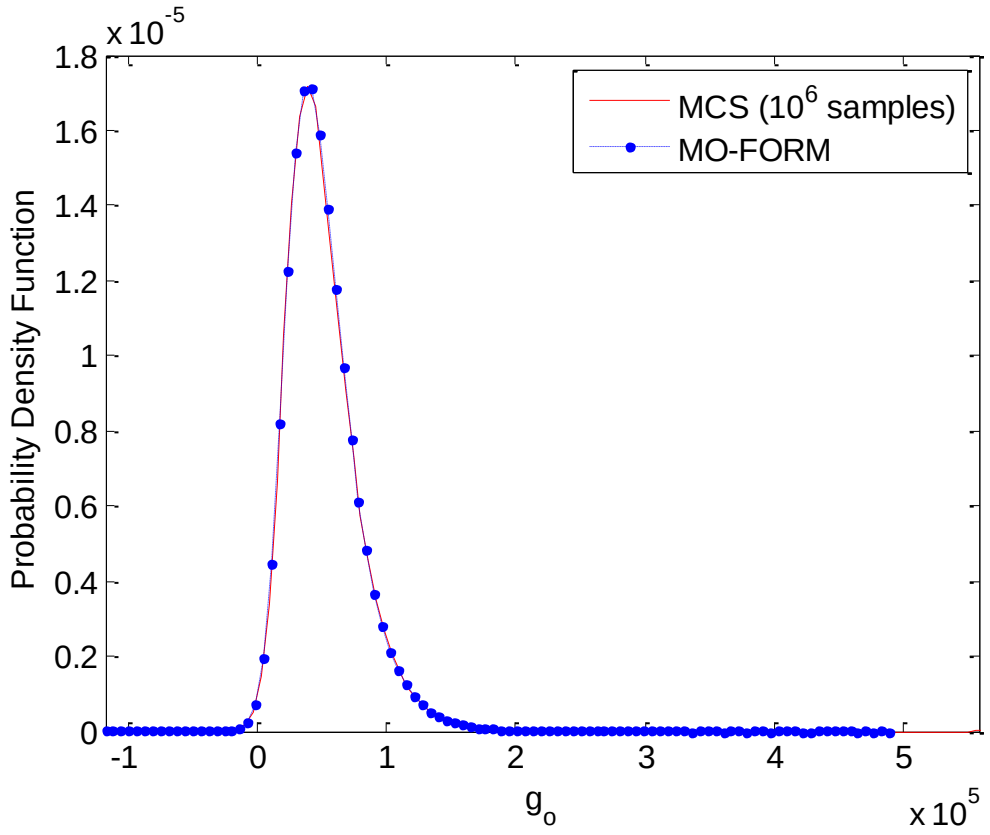

Figure 3.11: Pareto surface in the space of original random variables

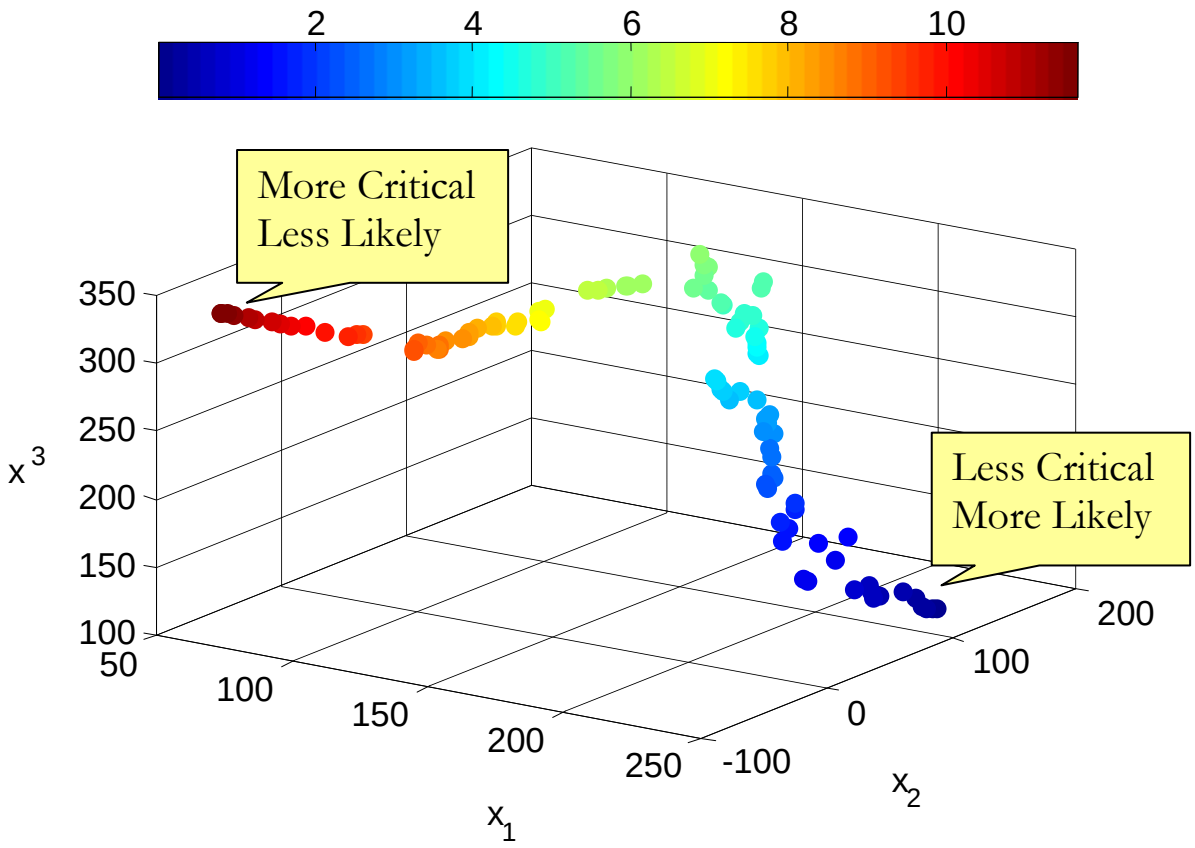

Figure 3.12: Planar truss example

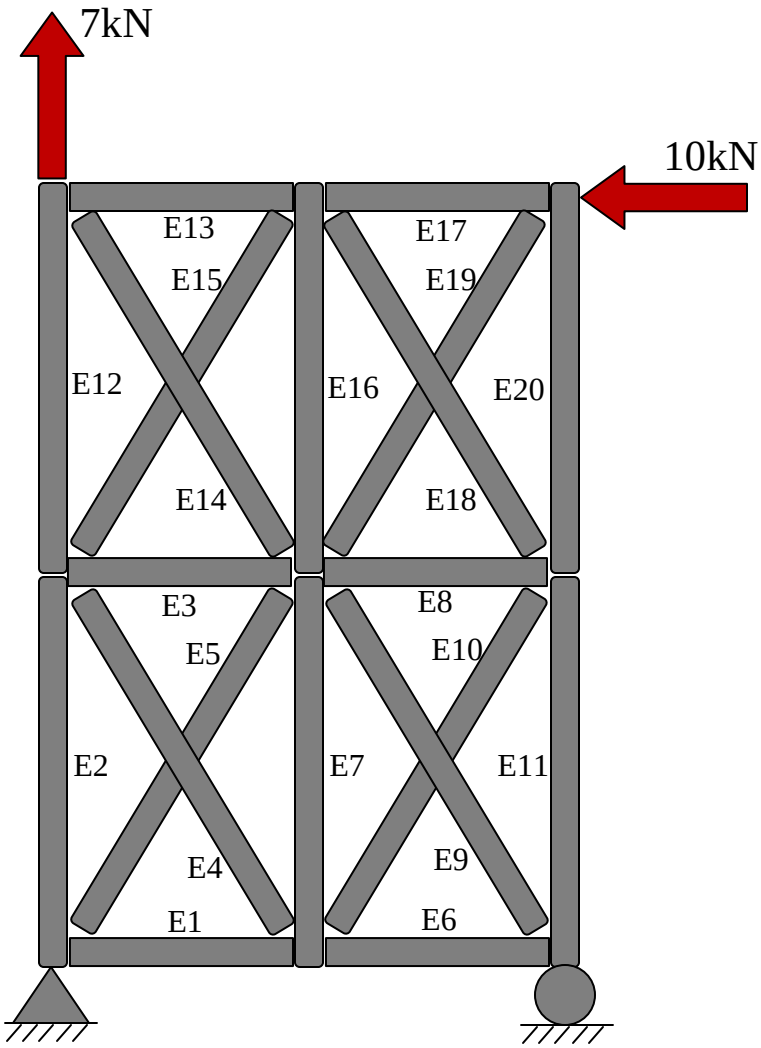

Figure 3.13 Pareto surface of the planar truss example for 500 in a population and 2000 generations

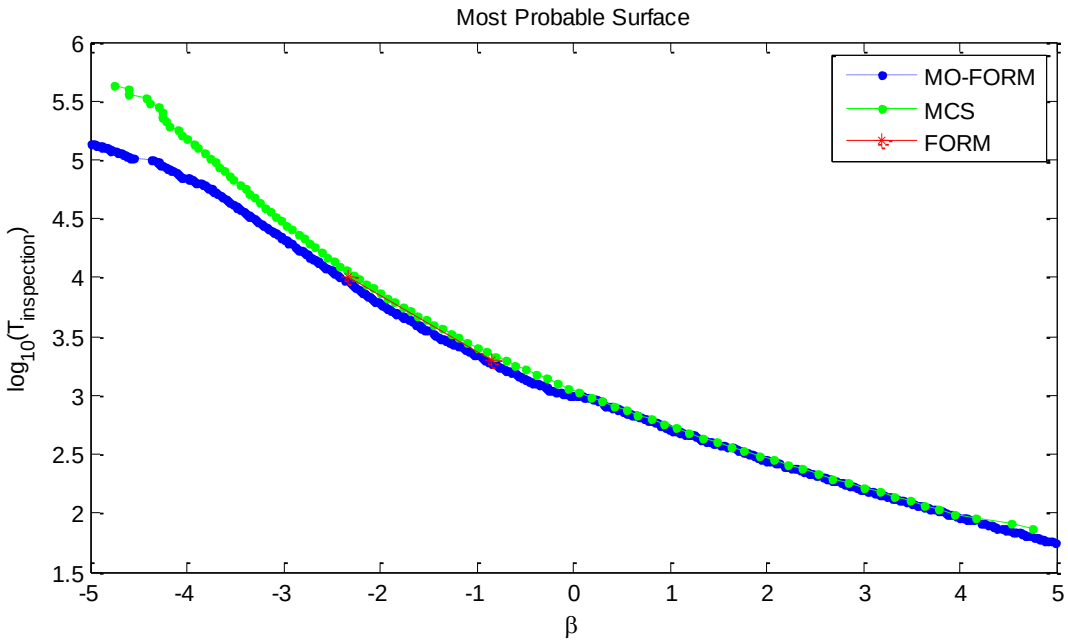

Figure 3.14: Pareto surface of the planar truss example for 1000 in a population and 1000 generations

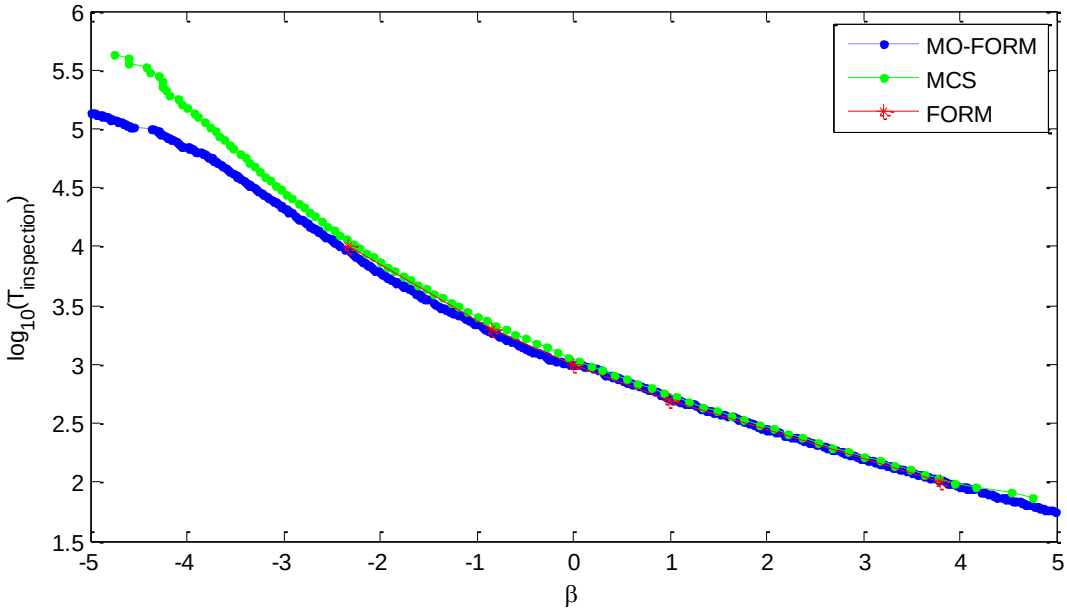

Figure 3.15: CDF of the planar truss example

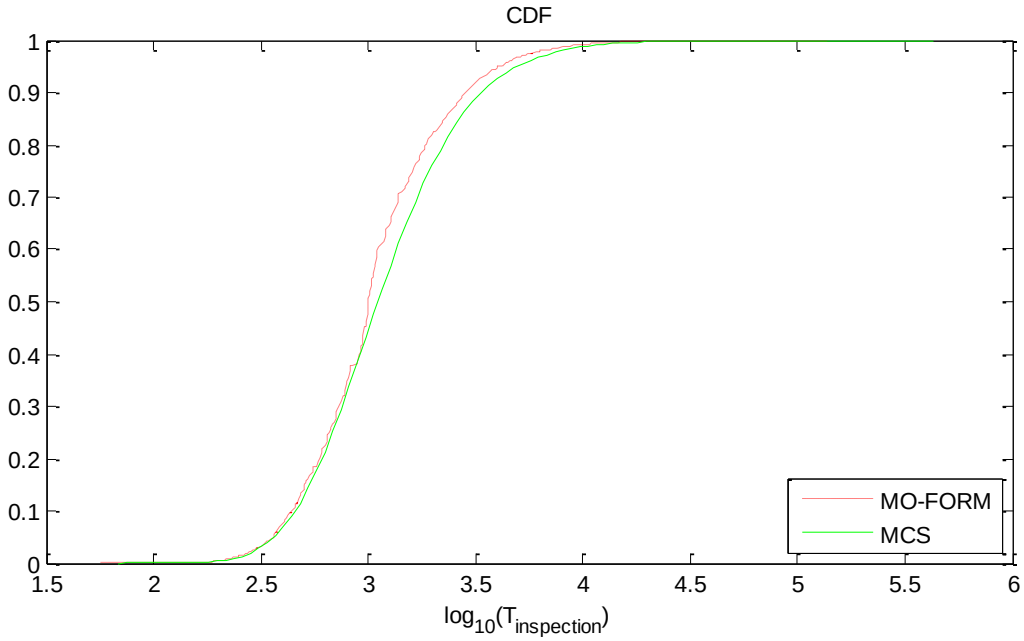

Figure 3.16: PDF of the planar truss example

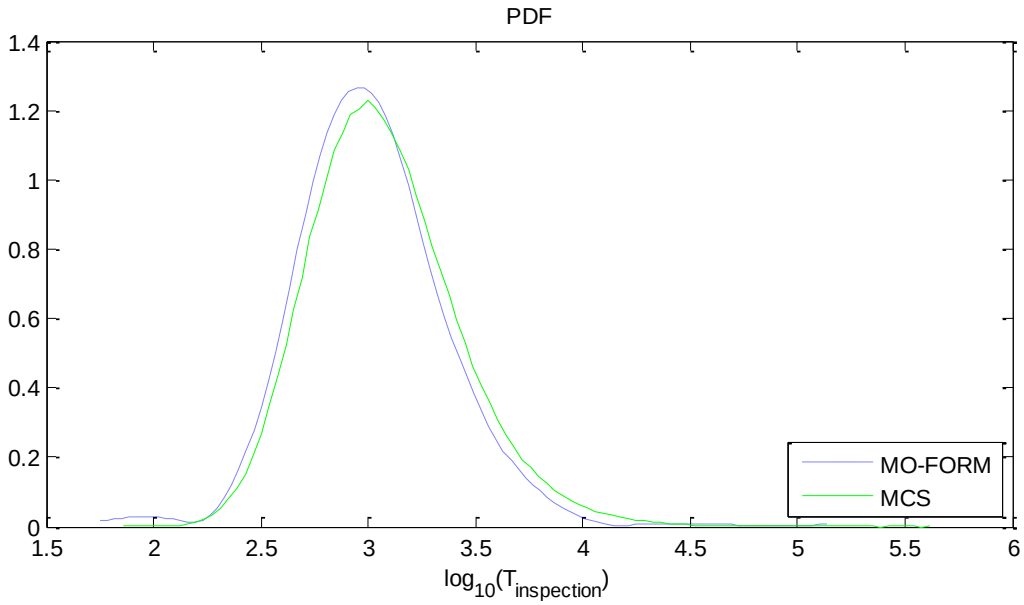

Figure 3.17: Relative importance measures for the planar truss example

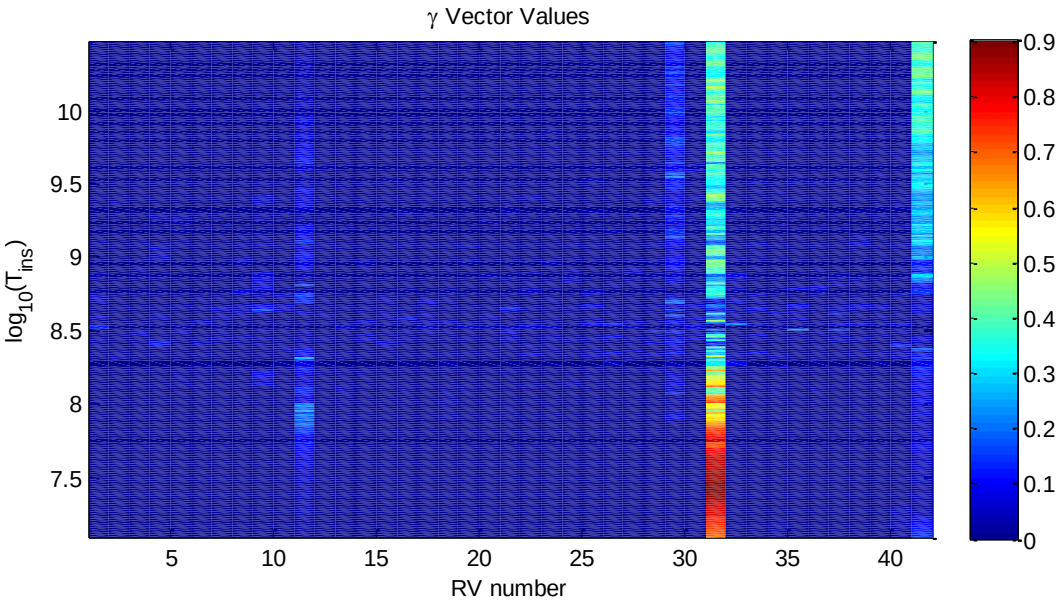

3.7 TABLES

Table 3.1. Distribution types and statistical parameters of random variables in first MO-FORM example

Random Variables	Distribution	Mean	Coefficient of Variation
$\mathbf{X_1}$	Lognormal	250	0.2
$\mathbf{X_2}$	Normal	100	$0.\overline{33}$
$\mathbf{X_3}$	Normal	120	$0.\overline{33}$

Table 3.2. Computational cost for the proposed method and MCS

	CPU time (seconds)
Proposed Method (1000 in a population)	**Total time: 8,093.9 sec (2.25 hrs)**
(500 in a population)	**7,528.9 sec (2.09 hrs)**
Crude-MCS	**Total time: 4,620.2 sec (1.28 hrs)**

CHAPTER 4

FUTURE WORK

Despite much effort to improve and implement the selective searching algorithm and MO-FORM, many areas remain for improvement. For the selective searching algorithm, the major issue remains that using a full MCS to find all failure mode probabilities causes this method to take too much computation time. Since FORM and SORM cannot be used to the high non-linearities of the limit state functions, a simulation method such as importance sampling must be used to properly find the failure probabilities. Since the design-point must be found for convenient importance sampling, one may expect the points or elite chromosome found by the selective searching method would correspond to these design points; however, this is not the case. Due to high non-linearities of the limit state functions, the failure modes are not identified at hypersphere radii that correspond to their overall reliability indices necessarily. With higher population numbers, this could be remedied, but this would also make the overall computational effort much higher without much improvement over crude-MCS. To remedy this, an inward searching algorithm can be developed to find the actual design point in the **u** space. This algorithm must be able to handle a highly non-linear and unknown path and have proper convergence criteria to be able to properly identify the design point. Since sampling can handle any type of non-linear function, this algorithm can generate points about a given point, and find the point that is still inside the limit state function and closest to the origin. Lastly, this algorithm must operate efficiently. The failure mode probability can then be effectively computed quickly by importance sampling.

For MO-FORM, systems with large numbers of variables must be better handled. As mentioned previously, with larger number of random variables, crude-MCS does not generate points that have magnitudes smaller than 5 due to a size effect, making it difficult to find an appropriate comparison for MO-FORM. FORM generally is not an appropriate comparison, as it is gradient based and can be fooled by local gradients during its search. More efficient sampling methods may be used to generate proper comparative Pareto surfaces from MCS. Once better comparisons are found, if it is determined that the Pareto surfaces found by MO-FORM are inappropriate, several paths can be pursued. The effect of stopping leeching may be investigated,

as NSGA-II uses this for every offspring population and this may cause premature convergence. Increasing the mutation probability may also decrease the possibility of premature convergence. Trying to increase the margins of the random variables may also help stop premature convergence, as NSGA-II requires minimum and maximum values of alleles in chromosomes to run properly. These, among other possible routes can be invested to improve both the selective searching method and MO-FORM.

CHAPTER 5

CONCLUSION

This work develops an efficient and accurate method to identify those cascading, fatigue-induced failure sequences that contribute most to the system failure probability and to calculate the probabilities of both the system failure as well as these individual failure sequences. With the proposed approach, the failure mode search and the system failure probability evaluation are decoupled. The proposed approach finds these failure modes using a genetic algorithm, characterizes these using a mutually exclusive formulation, and finally calculates each of these mode probabilities using a sampling method. From the mutually exclusive formulation, the system failure probability is calculated by summing the mode probabilities while accurately modeling dependence. The advantages from this approach are three-fold: decoupling failure mode identification and system reliability analysis helps to prevent the computational cost from rapidly increasing with structural complexity; a simulation-based, genetic algorithm inspired approach identified cascading fatigue-induced failure sequences; and using a mutually exclusive formulation for these cascading fatigue-induced failure sequences accurately models statistical dependence at all levels.

Since the proposed method relies on an *a priori* specified inspection cycle time, and this value is typically unknown before-hand, MO-FORM was developed to perform multiple FORM analyses simultaneously for many inspection cycle values.MO-FORM can find both the "less likely, but more critical" cases as well as the "more likely, but less critical" cases. Criticality is measured by a performance function, which is implemented as the time until failure for the fatigue-induced sequential failure cases, while likelihood is modeled by the reliability index values for solutions. Using NSGA-II, a robust multi-objective genetic algorithm that relies on rules of Pareto Optimality for assigning fitness function values in terms of fronts to each chromosome, a Pareto optimal surface can be found of values for both the time until failure and likelihood. After analysis, the PDF, CDF and statistical moments can be obtained for all levels of the performance function. MO-FORM presents many advantages: accurate modeling of both uncritical and likely events as well as critical but unlikely events; non-gradient based search; and finding relative importance measure of individual random variables at different levels of

inspection cycle times. The applicability of MO-FORM was then demonstrated for a simple, general case of three random variables. MO-FORM was then compared to MCS with one million samples and was shown to be accurate, especially for large and small values of the reliability indices.

Both methods were then demonstrated for system reliability analysis of complex numerical examples: the selective searching algorithm was used to analyze a 97 member planar-truss bridge with a full influence load analysis, and MO-FORM was used to analyze a 20 member planar-truss.. MCS then confirmed that the proposed method can compute the system failure probability accurately and efficiently. MO-FORM was confirmed by both FORM and MCS as modeling the full range of inspection cycle times accurately and efficiently.

Several possible improvements for future work were then proposed for both methods. For the selective searching algorithm, a method to search for the exact design point given a point in the failure mode domain was suggested. The failure mode probability could then be calculated using importance sampling about the found design point, replacing the need for a computationally costly crude-MCS for failure mode probability calculations. For MO-FORM, several improvements to the genetic operators and allele margins were proposed. Since crude-MCS is affected by problem scales and traditional FORM may be misled due to local gradients, it was also suggested that a better comparison for MO-FORM be developed. Once these proposed future improvements are developed, both methods will be greatly improved for general problems.

Both of these methods are strongly applicable for field practitioners. Using the selective searching algorithm for a given inspection cycle time, one can find the critical members that are the root of cascading fatigue induced failures and devote more attention to controlling damage and implementing repairs for these members. One can also find the most likely failure paths and be sure to stop cascading failures should component failures occur. To make better decisions about exact inspection cycle times, one can use MO-FORM to find the more likely but less critical cases and the less likely but more critical cases. From this information one can find the optimal inspection cycle time to prevent the likely cases and know what critical cases to be concerned with. One can then use the proposed importance measure scheme to find which

random variables contribute most to the system failure and control them through inspection and repair. For a more in-depth analysis, one could use the selective searching algorithms to find the critical failure modes. From these two methods, field practitioners can make better risk-informed decisions.

REFERENCES

AASHTO. 2004. *AASHTO LRFD Bridge Design Specifications*, 3rd Ed. AASHTO, Washington, D.C., USA.

Borrego L. P., Ferreira J. M., & Costa J. M. 2001. Fatigue crack growth and crack closure in an AlMgSi alloy. Blackwell Science Ltd. *Fatigue Fracture of Engineering Materials Structures*, 24: 255-265.

Cho, H.-N., Lim, J.-K. & Choi, H.-H. 2000. Reliability-based fatigue failure analysis for causes assessment of a collapsed steel truss bridge. *Engineering Failure Analysis* 8: 311-324.

Corotis, R.B. & Nafday, A.M. 1989. Structural system reliability using linear programming and simulation. *Journal of Structural Engineering* 115(10):2435-47.

Deb, K., and Agarwal, R.B. 1995. Simulated Binary Crossover for Continuous Search Space. *Complex Systems*, 9: 115-148.

Deb, K., Pratap, A., Agarwal, S., & Meyerivan, T. 2002. A Fast Elitist Multi-objective Genetic Algorithm: NSGA-II. *IEEE Transactions on Evolutionary Computation*, 6(2): 182 – 197.

Der Kiureghian, A. 2005. First- and second-order reliability methods. In E. Nikolaidis, Ghiocel, D.M. & Singhal, S. (eds.), *Engineering Design Reliability Handbook* CRC Press, Boca Raton, FL.

Der Kiureghian, A & Dakessian, T. 1998. Multiple design points in first and second-order reliability. *Structural Safety* 20(1): 37-49.

Der Kiureghian, A. & Song, J. 2008. Multi-scale reliability analysis and updating of complex systems by use of linear programming. *Reliability Engineering and System Safety* 93(2): 288-297.

Ditlevsen, O. 1979. Narrow reliability bounds for structural system. *Journal of Structural Mechanics* 7(4): 453-472.Ditlevsen, O. & Madsen, H.O. 1996. *Structural Reliability Methods*. Chichester, UK: John Wiley & Sons.

Feng, Y. 1989. A method for computing structural system reliability with high accuracy. *Computers & Structures* 33(1): 1-5.

Freudenthal, A.M, Garrelts, J.M. & Shinozuka, M. 1966. The analysis of structural safety. *Journal of Structures Division, ASCE* 92: 267-325.

Galambos, T.V. 1990. Systems reliability and structural design. *Structural Safety* 7: 101-108.

Gardoni, P., Der Kiureghian, A. and Mosalam, K. 2002. Probabilistic capacity models and fragility estimates for reinforced concrete columns based on experimental observations. *Journal of Engineering Mechanics* 128(10): 1024-1038.

Genz, A. 1992. Numerical computation of multivariate normal probabilities. *Journal of Computational and Graphical Stat.*: 141-149.

Goldberg, D.E. 1989. *Genetic algorithms in search, optimization and machine learning*. Reading (MA): Addison-Wesley.

Grimmelt, M. & Schueller, G.I. 1982. Benchmark study on methods to determine collapse failure probabilities of redundant structures. *Structural Safety* 1: 93-106.

Henwadi, S. & Frangopol, D.M. 1994. System reliability and redundancy in structural design and evaluation. *Structural Safety* 16: 47-71.

Holland, J.H. 1975. *Adaptation in natural and artificial systems*. University of Michigan Press, Ann Arbor, MI, USA.

Karamchandani, A. 1987. *Structural System Reliability Analysis Methods*. Report No. 83, Department of Civil Engineering, Stanford University.

Kim, D.-S. 2009. *Matrix-based System Reliability Analysis Using the Dominant Failure Mode Search Method*. Dept. of Civil and Environmental Engineering, Seoul National University, Seoul, Korea.

Korea Society of Civil Engineers (KSCE) 1995. Final report on precise safety inspection of Sung-Soo bridge, Seoul Metropolitan Government (in Korean).

Kurtz, N., Song, J. Kim, D.-S. & Ok, S.-Y. 2010. Multi-scale system reliability analysis of bridge structures using dominant failure modes identified by selective searching technique, *Proc. of IABMAS2010*, July 11-15, Philadelphia, PA, USA.

Lee, J.S. 1989. Basic study on the reliability analysis of structural systems. *Journal of Ocean Engineering and Technology* 3(2): 656-657.

Lee, Y.-J. & Song, J. 2010. Identification of critical sequences of fatigue-induced failures by branch-and-bound method employing system reliability bounds, *Proc. of AIAA SDM Conference*, April 12-15, Orlando, FL, USA.

Liu, N. & Tang, W.H. 2004. System reliability evaluation of nonlinear continuum structures – a probabilistic FEM approach. *Finite Elem. in Analysis and Design* 40: 595-610.

Liu, P.-L. & Der Kiureghian, A. 1986. Miltivariate distribution models with prescribed marginals and covariances. *Probabilistic Engineering Mechanics*, 1(2), 105-112.

McKay, N.J., Beckman, R.J. & Conover, W.J. 1979. A comparison of three methods for selecting value of input variables in the analysis of output from a computer code. *Technometrics* 21: 239-245.

Melchers, R.E. 1994. Structural system reliability assessment using directional simulation. *Structural Safety* 16: 23-37.

Melchers, R.E. 1999. *Structural Reliability: Analysis and Prediction*, 2nd edition. John Wiley, New York, NY, USA.

Moses, F. 1982. System reliability developments in structural engineering. *Structural Safety* 1(1): 3-13.

Moses, F. 1990. New directions and research needs in system reliability research. *Structural Safety* 7: 93-100.

Moses, F. & Stahl, B. 1978. Reliability analysis format for offshore structures. *Proceeding of the 10th Annual Offshore Technology Conference, Houston, Texas* Paper 3046.

Murotsu, Y., Okada, H., Taguchi, K., Grimmelt, M., & Yonezawa, M. 1984. Automatic generation of stochastically dominant failure modes of frame structures. *Structural Safety* 2:17-25.

National Transportation Safety Board (NTSB). 2008. *Collapse of I-35W Highway Bridge, Minneapolis, Minnesota, Ausugt 1, 2007.* Highway Accident Report NTSB/HAR-08/03. Washington, DC.

Newman, J. C. & Raju, I. S. 1981. An empirical stress intensity factor equation for the surface crack. *Engineering of Fracture Mechanics* 15: 185-193.

Paris, P.C. & Erdogan, F. 1963. A critical analysis of crack propagation laws. *J. Basic Eng., Trans. ASME* 85: 528-534.

Park, S.Y. 2001. A new methodology for the rapid calculation of system reliability of complex structures. *Architectural Research* 3(1): 71-80.

Ranganathan, R. & Deshpande, A.G. 1984. Generation of dominant modes and reliability analysis of frame. *Structural safety* 4:217-28.

Rashedi, M.R. 1983. *Studies on reliability of structural systems*. Department of Civil Engineering, Case Western Reserve University.

Shao, S. & Murotsu, Y. 1999. Approach to failure mode analysis of large structures. *Probabilistic Engineering Mechanics* 14: 169-177.

Shetty, N.K. 1994. Selective enumeration method for identification of dominant failure paths of large structures. *Proc. OMAE Conf., ASME, Safety and Reliability* 2: 381-391.

Song, J. & Der Kiureghian, A. 2003. Bounds on system reliability by linear programming. *Journal of Engineering Mechanics* 129(6): 627-636.

Song, J. & Kang, W.H. 2009. System reliability and sensitivity under statistical dependence by matrix-based system reliability method. *Structural Safety* 31(2): 148-156.

Song, J. & Ok, S.-Y. 2010. Multi-scale system reliability analysis of lifeline networks under earthquake hazards. *Earthquake Engineering & Structural Dynamics* 39(3): 259-279.

Srinivas, N. & Deb, K. 1994 Multiobjective optimization using nondominated sorting in genetic algorithms. *Evolutionary Computation*, 2(3):221-248.

Srividya, A. & Ranganathan, R. 1992. Automatic generation of stochastically dominant failure modes in frame structures for reliability studies. *Reliability Engineering and System Safety* 37: 15-23.

Thoft-Christensen, P. & Baker, M.J. 1982. *Structural Reliability Theory and its Applications*. Springer-Verlag.

Thoft-Christensen, P. & Murotsu, Y. 1986. *Application of Structural Systems Reliability Theory*. Springer-Verlag.

Xiao Q, & Mahadevan S. 1994. Fast failure mode identification for ductile structural system reliability. *Structural Safety* 13(4): 207-226.

Yarema, S. Y. 1982. Correlation of the parameters of the Paris equation and the cyclic crack resistance characteristics of materials. Plenum Publishing Corporation. 81(1309): 1090-1098.

Zhang, Y. & Der Kiureghian, A. 1995. Two improved algorithms for reliability analysis. In *Reliability and Optimization of Structural Systems*, Proceedings of the 6th IFIP WG 7.5

Working Conference on Reliability and Optimization of Structural Systems, 1994, (R. Rackwitz, G. Augusti, and A. Borri, Eds.), 297-304.

Zhao, Y.G. & Ono, T. 1998. System reliability evaluation of ductile frame structures. *Journal of Structural Engineering* 124(6): 678-685.

Zhou, Y. E. 2006. Assessment of bridge remaining fatigue life through field strain measurement. *Journal of Bridge Engineering* 11(6): 737-744.

AUTHOR'S BIOGRAPHY

Nolan Scot Kurtz received a Bachelor of Science in Civil Engineering from Carnegie Mellon University in May 2009. Starting in August of 2009, Kurtz has been pursuing research in the field of structural risk and reliability under the direction of Professor Junho Song at the University of Illinois at Urbana-Champaign. After finishing his Master of Science degree in Civil Engineering in December 2010, Kurtz will continue pursuing research in the same field under the direction of Professor Song.